Naval Research Laboratory

Stennis Space Center, MS 39529-5004

NRL/MR/7320--17-9738

Tests of Parameterized Langmuir-Circulation Mixing in the Ocean's Surface Mixed Layer II

Paul J. Martin

Ocean Dynamics and Prediction Branch
Oceanography Division

Ivan B. Savelyev

Coastal and Ocean Remote Sensing Branch
Remote Sensing Division

August 11, 2017

Approved for public release; distribution is unlimited.

REPORT DOCUMENTATION PAGE

Form Approved
OMB No. 0704-0188

Public reporting burden for this collection of information is estimated to average 1 hour per response, including the time for reviewing instructions, searching existing data sources, gathering and maintaining the data needed, and completing and reviewing this collection of information. Send comments regarding this burden estimate or any other aspect of this collection of information, including suggestions for reducing this burden to Department of Defense, Washington Headquarters Services, Directorate for Information Operations and Reports (0704-0188), 1215 Jefferson Davis Highway, Suite 1204, Arlington, VA 22202-4302. Respondents should be aware that notwithstanding any other provision of law, no person shall be subject to any penalty for failing to comply with a collection of information if it does not display a currently valid OMB control number. **PLEASE DO NOT RETURN YOUR FORM TO THE ABOVE ADDRESS.**

1. REPORT DATE *(DD-MM-YYYY)*	**2. REPORT TYPE**	**3. DATES COVERED** *(From - To)*
11-08-2017	Memorandum Report	

4. TITLE AND SUBTITLE

Tests of Parameterized Langmuir-Circulation Mixing in the Ocean's Surface Mixed Layer II

5a. CONTRACT NUMBER

5b. GRANT NUMBER

5c. PROGRAM ELEMENT NUMBER
0601153N

6. AUTHOR(S)

Paul J. Martin and Ivan B. Savelyev

5d. PROJECT NUMBER

5e. TASK NUMBER

5f. WORK UNIT NUMBER

7. PERFORMING ORGANIZATION NAME(S) AND ADDRESS(ES)

Naval Research Laboratory
Oceanography Division
Stennis Space Center, MS 39529-5004

8. PERFORMING ORGANIZATION REPORT NUMBER

NRL/MR/7320--17-9738

9. SPONSORING / MONITORING AGENCY NAME(S) AND ADDRESS(ES)

Office of Naval Research
One Liberty Center
875 North Randolph Street, Suite 1425
Arlington, VA 22203-1995

10. SPONSOR / MONITOR'S ACRONYM(S)

ONR

11. SPONSOR / MONITOR'S REPORT NUMBER(S)

12. DISTRIBUTION / AVAILABILITY STATEMENT

Approved for public release; distribution is unlimited.

13. SUPPLEMENTARY NOTES

14. ABSTRACT

Recent large-eddy simulations (LES) of Langmuir circulation (LC) within the surface mixed layer (SML) of the ocean found that LC can significantly increase the rate of mixing within the SML and sometimes increase the mixed layer depth (MLD). This report investigates the parameterization of the effects of LC on upper-ocean mixing presented in Kantha and Clayson (2004) and Harcourt (2015). These parameterizations of the enhancement of upper-ocean mixing by LC were implemented in the version of the Mellor-Yamada Level 2.5 (MYL2.5) turbulence model used in the Navy Coastal Ocean Model (NCOM) and tested for (a) a simple wind-mixing case, (b) simulations of the upper ocean thermal structure at Ocean Weathership Station (OWS) Papa, and (c) simulations of Hurricane Ivan in the Gulf of Mexico. Results with the Kantha and Clayson (2004) and Harcourt (2015) LC mixing parameterizations are compared with each other and with NCOM's original MYL2.5 turbulence model without a LC mixing parameterization.

15. SUBJECT TERMS

Surface mixed layer — Langmuir circulation
Ocean turbulence — Ocean modeling

16. SECURITY CLASSIFICATION OF:			**17. LIMITATION OF ABSTRACT**	**18. NUMBER OF PAGES**	**19a. NAME OF RESPONSIBLE PERSON**
a. REPORT	**b. ABSTRACT**	**c. THIS PAGE**			Paul Martin
Unclassified Unlimited	Unclassified Unlimited	Unclassified Unlimited	Unclassified Unlimited	52	**19b. TELEPHONE NUMBER** *(include area code)* (228) 688-5447

Standard Form 298 (Rev. 8-98)
Prescribed by ANSI Std. Z39.18

CONTENTS

TESTS OF PARAMETERIZED LANGMUIR-CIRCULATION MIXING IN THE OCEAN'S SURFACE MIXED LAYER II

1. INTRODUCTION

It has long been assumed that Langmuir circulation (LC) affects mixing in the ocean's surface mixed layer (SML), but until computing power had advanced sufficiently to allow large-eddy simulations (LES) of LC, there was not much quantitative information upon which to base a parameterization of the effects of LC mixing in ocean models.

However, beginning in the 1990's, LES began being used to investigate LC and its effects on upper-ocean mixing. Some papers on this research include Skyllingstad and Denbo (1995), McWilliams et al. (1997, hereafter referred to as MW97), Skyllingstad et al. (1999), Skyllingstad (2000), McWilliams and Sullivan (2000), Min and Noh (2004), Noh et al. (2004), Sullivan et al. (2004), Harcourt and D'Asaro (2007), Tejada-Martinez and Grosch (2007), Polton and Belcher (2007), Sullivan et al. (2007), Grant and Belcher (2009), Kukulka et al. (2009), Alan et al. (2009), Li et al. (2009), Tejada-Martinez et al. (2009), Martinat et al. (2011), Sullivan et al. (2012), Van Roekel et al. (2012), and Hamlington et al. (2014).

MW97 conducted LES simulations of LCs for a simple, wind-mixing case with an initial mixed-layer depth (MLD) of about 33 m and a moderate wind of about 5 m/s. They found that the inclusion of LCs in their LES increased the rate of mixing within the SML by about a factor of 3 and slightly increased the depth of mixing.

Based on these results from MW97, Kantha and Clayson (2004, hereafter referred to as KC04) investigated how to implement the increased rate of mixing by the LC in the widely-used Mellor-Yamada Level 2.5 (MYL2.5) turbulence model (Mellor 1974, Mellor and Yamada 1982). They added additional shear-production terms to the MYL2.5 model, consisting of the product of the vertical Reynolds stress multiplied by the vertical shear of the Stokes drift current (SDC) from the waves. The additional shear-production terms were added to both the turbulent kinetic energy (TKE) equation and the turbulence length-scale (TLS) equation of the MYL2.5 model. For the conditions of the simple, wind-mixing simulation conducted by MW97, KC04's modifications significantly increased the maximum rates of mixing in the SML, and the higher mixing rates were fairly consistent with the LES results of MW97.

Martin et al. (2013, hereafter referred to as M13) described the implemetation of KC04's parameterization of LC mixing in the version of the MYL2.5 turbulence model that is used in the Navy Coastal Ocean Model (NCOM) and the results of a number of tests of the implementation of the KC04 parameterization in NCOM. The tests included the simple, wind-mixing test case used by MW97 and KC04, a year-long simulation of the SML at Ocean Weathership Station (OWS)

Manuscript approved October 10, 2016.

Papa in the NE Pacific, and a simulation of the effect of Hurricane Ivan on the upper ocean in the Gulf of Mexico in 2004. The results were found to be consistent with those reported by KC04 in that their parameterization of LC mixing in the MYL2.5 turbulence model increased the rate of mixing within the SML by a factor of 2-3 and slightly increased the depth of mixing, and was otherwise well behaved and numerically robust.

Since the KC04 paper, there have been additional efforts to parameterize the effects of LC on upper-ocean mixing in turbulence models. Two notable efforts are those by Harcourt (2013 and 2015). Harcourt noted that the stability functions used in KC04 were derived from the algebraic Reynolds stress model (ARSM) used in Kantha and Clayson (1994, hereafter referred to as KC94) that included the effects of local stratification and shear, but not the Craik-Leibovitch (CL) vortex force (Craik and Leibovich 1976), and that this was inconsistent with KC04's use of the CL vortex force to derive modifications to the prognostic equations for predicting the TKE and the TLS. Hence, Harcourt included the CL vortex force in all the ARSM equations used to determine the effect of LC on both the stability functions and the TKE and TLS equations.

In this report, the implementations in NCOM's MYL2.5 turbulence model of the parameterization of LC mixing by Kantha and Clayson (2004) and by Harcourt (2015, hereafter referred to as H15) are described, and the results of some tests are reported, including comparisons with NCOM's original MYL2.5 turbulence model without a parameterization of LC mixing. Hence, this report is a follow on to the discussion of the KC04 parameterization of LC mixing in M13.

The following sections contain a description of the implementation of both the KCO4 and the H15 Langmuir Circulation mixing parameterizations (LCMPs) in the MYL2.5 turbulence model used in NCOM (Section 2), a test of the KC04 and H15 LCMPs for the simple, wind-mixing, test case used by MW97 and KC04 (Section 3), a test of the KC04 and H15 LCMPs at OWS Papa (Section 4), a test of the KC04 and H15 LCMPs for a simulation of Hurricane Ivan in the Gulf of Mexico (Section 5), and a summary (Section 6).

2. IMPLEMENTATION OF LC MIXING IN THE MYL2.5 MLM

2.1 Original MYL2.5 MLM in NCOM

The original TKE and TLS equations as implemented in the MYL2.5 MLM used in NCOM are

$$\frac{\partial q^2}{\partial t} = -\nabla\cdot(\mathbf{v}q^2) + Qq^2 + \nabla_h(A_H\nabla_h q^2) + \frac{\partial}{\partial z}\left(K_q\frac{\partial q^2}{\partial z}\right) + 2K_M\left(\left(\frac{\partial u}{\partial z}\right)^2 + \left(\frac{\partial v}{\partial z}\right)^2\right) + 2K_H\frac{g}{\rho_o}\frac{\partial\tilde{\rho}}{\partial z} - 2\frac{q^3}{b_1\ell}, \tag{1}$$

$$\frac{\partial q^2\ell}{\partial t} = -\nabla\cdot(\mathbf{v}q^2\ell) + Qq^2\ell + \nabla_h(A_H\nabla_h(q^2\ell)) + \frac{\partial}{\partial z}\left(K_q\frac{\partial q^2\ell}{\partial z}\right) + E_1\ell K_M\left(\left(\frac{\partial u}{\partial z}\right)^2 + \left(\frac{\partial v}{\partial z}\right)^2\right) + E_3\ell K_H\frac{g}{\rho_o}\frac{\partial\tilde{\rho}}{\partial z} - E_2\frac{q^3}{b_1}W, \tag{2}$$

where q is the square root of twice the TKE, ℓ is the turbulent length scale, t is the time, $\mathbf{v}$ is the vector velocity, Q is a volume flux source term, A_H is the horizontal mixing coefficient, z is

the vertical coordinate, K_q is the vertical diffusion coefficient for q^2 and $q^2\ell$, which is taken to be proportional to K_M ($K_q = 0.41K_M$), K_M is the vertical mixing coefficient for momentum, u and v are the horizontal components of the velocity, K_H is the vertical diffusion coefficient for scalar fields, g is the acceleration of gravity, ρ_o is a reference density for the water, and $\partial\tilde{\rho}/\partial z$ is the vertical gradient of the water density, with the contribution of the pressure to the vertical density gradient removed.

W is referred to by Mellor and Yamada (1982) as a "wall proximity" function, which is used to scale ℓ near the surface and bottom. This function is defined by

$$W = 1 + E_4 \left(\frac{\ell}{\kappa L}\right)^2, \tag{3}$$

and in NCOM, L is defined by

$$L^{-1} = (\zeta - z + z_s)^{-1} + (z - H + z_b)^{-1}, \tag{4}$$

where $\kappa = 0.4$ is Von Karman's constant, ζ is the elevation of the free surface, z_s is the surface roughness, z_b is the bottom roughness, and H is the static bottom depth. The symbols b_1, E_1, E_2, E_3, and E_4 are constants, with values specified in Table 1.

Table 1 — Constants for MYL2.5 Turbulence Equations used in NCOM

parameter	*value*
a_1	0.92
b_1	16.6
a_2	0.74
b_2	10.1
c_1	0.08
E_1	1.8
E_2	1.0
E_3	1.8
E_4	1.33

The vertical mixing coefficients K_M and K_H are computed as

$$K_M = \ell q S_M, \tag{5}$$

$$K_H = \ell q S_H, \tag{6}$$

where S_M and S_H are "stability functions" computed as

$$S_H = \frac{C_1}{1 - C_2 G_H}, \tag{7}$$

$$S_M = \frac{C_3 + C_4 G_H S_H}{1 - C_5 G_H}, \tag{8}$$

where

$$G_H = \min\left[0.028, \frac{\ell^2 g}{q^2 \rho_o}\frac{\partial \tilde{\rho}}{\partial z}\right]. \tag{9}$$

The constants C_1 – C_5 are calculated from the basic turbulence constants (a_1, a_2, b_1, b_2, and c_1) as

$$C_1 = a_2(b_1 - 6a_1)/b_1, \tag{10}$$

$$C_2 = a_2(18a_1 + 3b_2), \tag{11}$$

$$C_3 = a_1(b_1(1 - 3c_1) - 6a_1)/b_1, \tag{12}$$

$$C_4 = a_1(18a_1 + 9a_2), \tag{13}$$

$$C_5 = 9a_1a_2. \tag{14}$$

Table 1 lists the values of the constants used in the MYL2.5 turbulence model in NCOM.

2.2 Implementation of KC04 parameterization of LC mixing in MYL2.5 MLM

KC04 parameterized the effects of the LC mixing from the LES conducted by MW97 by adding additional shear production terms to both the TKE and TLS equations in the MYL2.5 turbulence model. The TKE and TLS equations in NCOM with the additional shear production terms used by KC04 are

$$\begin{aligned}\frac{\partial q^2}{\partial t} = &-\nabla\cdot(\mathbf{v}q^2) + Qq^2 + \nabla_h(A_H\nabla_h q^2) + \frac{\partial}{\partial z}\left(K_q\frac{\partial q^2}{\partial z}\right)\\ &+ 2K_M\left(\left(\frac{\partial u}{\partial z}\right)^2 + \left(\frac{\partial v}{\partial z}\right)^2 + \frac{\partial u}{\partial z}\frac{\partial u_s}{\partial z} + \frac{\partial v}{\partial z}\frac{\partial v_s}{\partial z}\right) + 2K_H\frac{g}{\rho_o}\frac{\partial\tilde{\rho}}{\partial z} - 2\frac{q^3}{b_1\ell},\end{aligned} \tag{15}$$

$$\begin{aligned}\frac{\partial q^2\ell}{\partial t} = &-\nabla\cdot(\mathbf{v}q^2\ell) + Qq^2\ell + \nabla_h(A_H\nabla_h(q^2\ell)) + \frac{\partial}{\partial z}\left(K_q\frac{\partial q^2\ell}{\partial z}\right)\\ &+ E_1\ell K_M\left(\left(\frac{\partial u}{\partial z}\right)^2 + \left(\frac{\partial v}{\partial z}\right)^2\right) + E_6\ell K_M\left(\frac{\partial u}{\partial z}\frac{\partial u_s}{\partial z} + \frac{\partial v}{\partial z}\frac{\partial v_s}{\partial z}\right)\\ &+ E_3\ell K_H\frac{g}{\rho_o}\frac{\partial\tilde{\rho}}{\partial z} - E_2\frac{q^3}{b_1}W,\end{aligned} \tag{16}$$

where u_s and v_s are the horizontal components of the SDC from the waves. An additional constant E_6 is used to scale the Stokes shear production term in the TLS equation and has a value of 7.2. Note that the value of 7.2 for E_6 is different from the value of 4.0 reported in KC04, which was incorrect (Dr. Lakshmi Kantha, personal communication). We found in early testing that the KC04 LC mixing parameterization does not work correctly (i.e., as reported by KC04) with $E_6 = 4.0$.

The original shear-production terms are proportional to the square of the vertical shear of the Eulerian velocity u and v; hence, the original shear-production terms are always positive and

always act to increase the TKE. The shear-production terms added by KC04 to parameterize the LC mixing include the vertical shear of the model Eulerian velocity times the vertical shear of the SDC; hence, it is possible for this term to be negative if the two velocity shears are of different sign, which would result in a loss of TKE from this term, rather than a gain. In tests conducted to date, this term is usually positive when the winds and wave directions are approximately alligned. When the winds and waves are in significantly different directions, this term can be negative and, hence, act to reduce the amount of mixing. A reduction in the vertical mixing with increasing misallignment of the wind and wave directions has been shown to occur in LES (Van Roekel et al. 2012). Preliminary tests with the KC04 (e.g., Carniel et al. 2005) and H15 LCMPs have also shown a reduction in vertical mixing with increasing misallignment of the wind and waves, though determination of the extent of the agreement of the LCMPs with the LES in this regard needs further investigation.

The vertical mixing coefficients and stability functions are computed using the equations described in the previous section. The constants used by KC04 are the same as those listed in Table 1 in the previous section, except that $E_4 = 4.87$.

2.3 Implementation of H15 parameterization of LC mixing in MYL2.5 MLM

The derivation of H15's parameterization of the effects of LC on upper-ocean mixing can be found in Harcourt (2015). What will be described here is the implementation of the H15 parameterization of LC mixing in NCOM.

H15's inclusion of the CL vortex force in the ARSM equations results in a modified form of the vertical turbulent momentum flux, i.e.,

$$-\overline{u'w'} = K_M \frac{\partial u}{\partial z} + K_M^S \frac{\partial u_s}{\partial z}, \tag{17}$$

$$-\overline{v'w'} = K_M \frac{\partial v}{\partial z} + K_M^S \frac{\partial v_s}{\partial z}, \tag{18}$$

where the second term on the right-hand side (RHS) of these two equations represents a vertical turbulent momentum flux down the gradient of the Stoke's current proportional to the vertical mixing coefficient K_M^S. This additional term, which does not appear in the KC04 parameterization, affects the momentum equations for u and v, as well as the shear production terms in the TKE and TLS equations. When the momentum equations are solved, this additional term acts as an explicit forcing term on the RHS of the momentum equations.

The TKE and TLS equations with the additional shear production terms derived by H15, including the modified vertical momentum flux, are

$$\begin{aligned}\frac{\partial q^2}{\partial t} = &-\nabla\cdot(\mathbf{v}q^2) + Qq^2 + \nabla_h(A_H\nabla_h q^2) + \frac{\partial}{\partial z}\left(K_q\frac{\partial q^2}{\partial z}\right)\\ &+ 2\left(\left(K_M\frac{\partial u}{\partial z} + K_M^S\frac{\partial u_s}{\partial z}\right)\left(\frac{\partial u}{\partial z} + \frac{\partial u_s}{\partial z}\right) + \left(K_M\frac{\partial v}{\partial z} + K_M^S\frac{\partial v_s}{\partial z}\right)\left(\frac{\partial v}{\partial z} + \frac{\partial v_s}{\partial z}\right)\right)\\ &+ 2K_H\frac{g}{\rho_o}\frac{\partial\tilde{\rho}}{\partial z} - 2\frac{q^3}{b_1\ell},\end{aligned} \tag{19}$$

$$\frac{\partial q^2\ell}{\partial t} = -\nabla\cdot(\mathbf{v}q^2\ell) + Qq^2\ell + \nabla_h(A_H\nabla_h(q^2\ell)) + \frac{\partial}{\partial z}\left(K_q\frac{\partial q^2\ell}{\partial z}\right) + E_1\ell\left(\left(K_M\frac{\partial u}{\partial z} + K_M^S\frac{\partial u_s}{\partial z}\right)\frac{\partial u}{\partial z} + \left(K_M\frac{\partial v}{\partial z} + K_M^S\frac{\partial v_s}{\partial z}\right)\frac{\partial v}{\partial z}\right) + E_6\ell\left(\left(K_M\frac{\partial u}{\partial z} + K_M^S\frac{\partial u_s}{\partial z}\right)\frac{\partial u_s}{\partial z} + \left(K_M\frac{\partial v}{\partial z} + K_M^S\frac{\partial v_s}{\partial z}\right)\frac{\partial v_s}{\partial z}\right) + E_3\ell K_H\frac{g}{\rho_o}\frac{\partial\tilde{\rho}}{\partial z} - E_2\frac{q^3}{b_1}W. \tag{20}$$

The vertical mixing coefficients are computed as

$$K_M = \ell q S_M, \tag{21}$$

$$K_H = \ell q S_H, \tag{22}$$

$$K_M^S = \ell q S_M^S f_z, \tag{23}$$

$$K_q = 0.41 K_H, \tag{24}$$

where f_z is a "surface proximity function", which is an empirical function chosen by H15 to reduce values near the surface in order to improve agreement with observations.

The stability functions are computed as

$$S_M^S = \frac{C_1}{1 - C_2G_H - C_3G_Vf_z}, \tag{25}$$

$$S_H = \frac{C_{11} - C_{12}G_H + C_{13}G_Sf_z^2 - C_{14}G_vf_z}{(1 - C_{15}G_H - C_{16}G_Vf_z)(1 - C_{17}G_H) - (C_{18} + C_{19}G_Hf_z - C_{20}G_Vf_z)G_Vf_z}, \tag{26}$$

$$S_M = \frac{C_{31} + C_{32}G_HS_H + C_{33}G_Sf_z^2S_M^S}{1 - C_{34}G_H - C_{35}G_Vf_z}, \tag{27}$$

where

$$G_H = \left(\frac{\ell}{q}\right)^2\frac{g}{\rho_o}\frac{\partial\tilde{\rho}}{\partial z}, \tag{28}$$

$$G_V = \left(\frac{\ell}{q}\right)^2\left(\frac{\partial u}{\partial z}\frac{\partial u_s}{\partial z} + \frac{\partial v}{\partial z}\frac{\partial v_s}{\partial z}\right), \tag{29}$$

$$G_S = \left(\frac{\ell}{q}\right)^2\left(\left(\frac{\partial u_s}{\partial z}\right)^2 + \left(\frac{\partial v_s}{\partial z}\right)^2\right). \tag{30}$$

The surface proximity function f_z is computed as

$$f_z = \tanh(C_\ell^S z/\ell^S), \tag{31}$$

where

$$\ell^S = \frac{\int_z \ell P_+^S dz}{\int_z P_+^S dz}, \tag{32}$$

where $C_\ell^S = 0.25$, $P_+^S = \max(0,P)$, and P is the Stokes shear production term

$$P = -\overline{u'w'}\frac{\partial u_s}{\partial z} - \overline{v'w'}\frac{\partial v_s}{\partial z}, \tag{33}$$

which is computed as

$$P = \ell q \left(\left(S_M \frac{\partial u}{\partial z} + S_M^S \frac{\partial u_s}{\partial z} \right) \frac{\partial u_s}{\partial z} + \left(S_M \frac{\partial v}{\partial z} + S_M^S \frac{\partial v_s}{\partial z} \right) \frac{\partial v_s}{\partial z} \right). \tag{34}$$

The surface proximity function is small (but positive) near the surface and increases to a value of one within the SML.

Because of the dependence of the surface proximity function f_z on the stability functions, the calculation of f_z and the stability functions is iterated a few times (5 times in the simulations conducted for this report) to obtain approximate convergence. The order of these calculations in NCOM is roughly the inverse of the order of the equations above, i.e., (34), (32), (31), (28-30), and (25-27). After the stability functions are computed, new values of the vertical mixing coefficients (21-23) can be calculated.

The form of the stability functions presented in H15 involves more constants than those presented in (25-28). Equations (25-28) are the calculations used in NCOM and represent the maximum reduction of H15's stability functions that can be obtained by combining constants. Relations between the constants used in H15 and those in (25-28) are presented in Table 3.

The complexity of H15's stability functions allows for the possibility of unreasonable or unstable behavior, e.g., the denominators of (25-28) could possibly go to zero. Hence, as noted in H15, some "realizability constraints" are needed to maintain reasonable values and avoid numerical instability. Since no guidance regarding realizability constraints were included in H15, the following constraints were implemented in NCOM based on some trial calculations: the maximum value of G_H was limited to 0.032, the denominators of (25-28) were restricted to minimum values of 0.01, and the stability functions themselves were limited to values in the range of 0 to 5. Also, the vertical mixing coefficients (25-27) were limited to the range of 0–10 m^2/s. Note that not a lot of time was spent investigating this; hence, these constraints could no doubt be improved.

The values of the constants used by H15 are listed in Tables 2 and 3. Note that $E_3 = 5.0$ instead of 1.8 as used in KC04 and $E_6 = 6.0$ instead of 7.2.

The behavior of the H15 turbulence parameterization when the SDC is zero is of interest, since the SDC in the SML will be small when the waves are small, and will be zero in deep mixed layers below the influence of the surface waves. When the SDC is zero, the G_V and G_S functions ((29) and (30)) will be zero, and the stability functions S_H and S_M become

Table 2 — Constants for Turbulence Equations for H15

parameter	*value*
a_1	0.92
b_1	16.6
a_2	0.74
b_2	10.1
c_1	0.08
c_2	0.7
c_3	0.2
E_1	1.8
E_2	1.0
E_3	5.0
E_4	1.33
E_6	6.0

Table 3 — Constants for Stability Functions for H15

parameter	*value*	*equivalent base turbulence constants*
γ_1	0.667470	$1 - 6a_1/b_1$
C_1	0.614072	$a_1\gamma_1$
C_2	6.127200	$9a_1a_2$
C_3	7.617600	$9a_1^2$
C_{11}	0.493928	$a_2\gamma_1$
C_{12}	3.026394	$9a_1a_2^2\gamma_1$
C_{13}	10.551480	$9a_1a_2\gamma_1(2a_1 + a_2)$
C_{14}	8.292656	$9a_1a_2(2a_1(\gamma_1 + 3c_1) - a_2(\gamma_1 - 3c_1))$
C_{15}	6.127200	$9a_1a_2$
C_{16}	30.470400	$36a_1^2$
C_{17}	30.192001	$3a_2(6a_1 + b_2(1 - c_3))$
C_{18}	1.478520	$9a_2^2(1 - c_2)$
C_{19}	284.308960	$162a_1^2a_2(2a_1 + a_2(2 - c_2))$
C_{20}	45.051102	$324a_1^2a_2^2(1 - c_2)$
C_{31}	0.393272	$a_1(\gamma_1 - 3c_1)$
C_{32}	17.073360	$9a_1(2a_1 + a_2(1 - c_2))$
C_{33}	22.852800	$27a_1^2$
C_{34}	6.127200	$9a_1a_2$
C_{35}	30.470400	$36a_1^2$

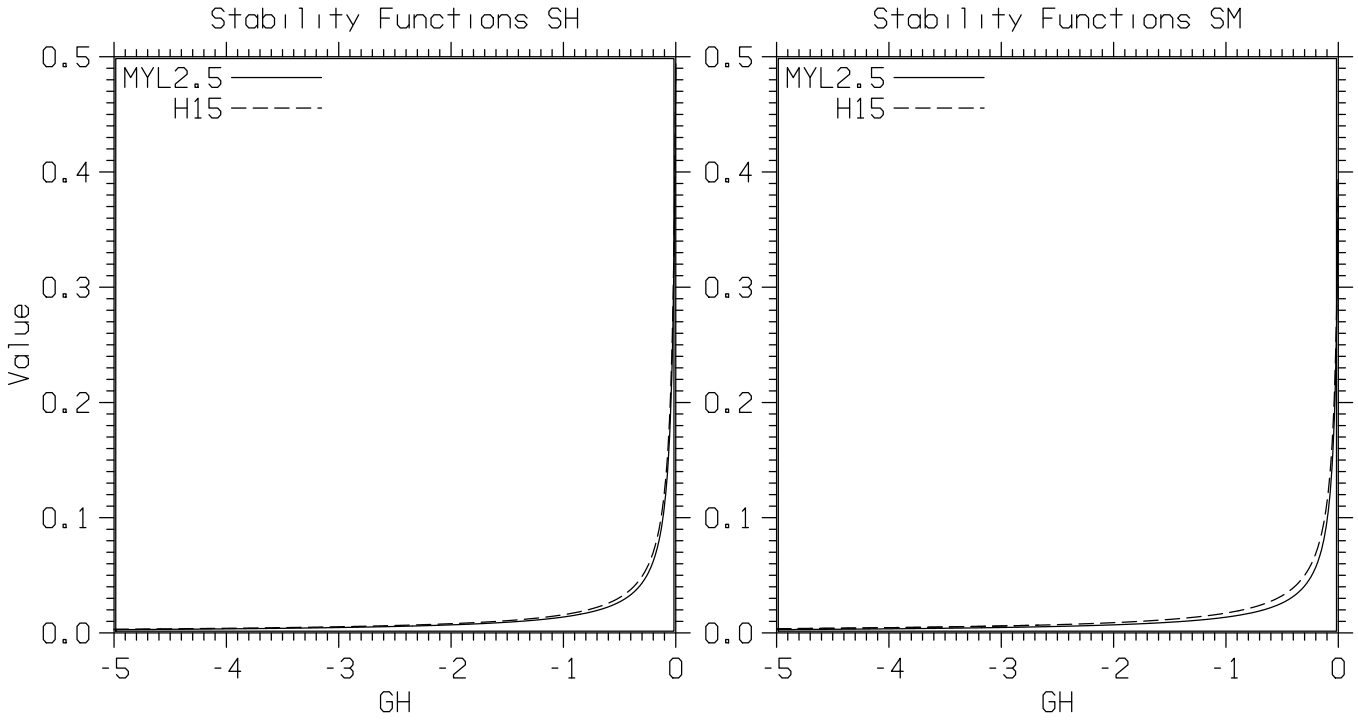

Fig. 1 — Plots of stability functions for MYL2.5 and H15 with SDC set to zero.

$$S_H = \frac{C_{11} - C_{12} G_H}{(1 - C_{15} G_H)(1 - C_{17} G_H)}, \tag{35}$$

$$S_M = \frac{C_{31} + C_{32} G_H S_H}{1 - C_{34} G_H}. \tag{36}$$

These can be compared with the stability functions for the MYL2.5 MLM in (7) and (8). The equations for S_M, (8) and (36), have the same form and the constants are the same except for C_4 for MYL2.5 and C_{32} for H15, which though different are somewhat similar in value, i.e., 21.36 and 17.07, respectively. The equations for S_H, (7) and (35) have slightly different forms, but the constants are such that the function values are similar. This is illustrated in Fig. 1, which shows plots of S_H and S_M for MYL2.5 and for H15 with the SDC set equal to zero. Hence, it might be expected that when the SDC is zero, H15 will predict vertical mixing similar to MYL2.5; this is demonstrated in Section 4.4 in simulations at OWS Papa.

2.4 Additional changes to NCOM to accommodate wave forcing

The coupling of NCOM with the output from a wave model requires some additional changes besides enhancing the vertical mixing within the MYL2.5 turbulence model. The SDC is added to NCOM's Coriolis term as described by MW97 and KC04 and many others. This term is referred to as the Stokes-Coriolis term and it affects the downwind transport in the surface wind-driven layer as discussed in MW97 and KC04 and in this report in the next section. The SDC is also used to advect the model fields in NCOM and, to be consistent with this advection, is added to NCOM's continuity equation. Note that the addition of the SDC to NCOM's Coriolis terms affects local, one-dimensional simulations, such as those presented in this report, but the advection by the SDC does not.

Additional wave effects include the surface wave-radiation stress, which is implemented in NCOM similar to the surface wind stress; but since it is generally much smaller than the wind stress, its effect is usually small, though not negligible. Another effect of the waves is the enhancement of bottom drag in shallow water due to the orbital motions of the surface-waves near the bottom (Grant and Madsen 1979; Soulsby 1995). Both of these additional wave-forcing effects are implemented in NCOM, but these effects are not the focus of this study and will not be discussed further in this report.

3. TEST OF LC MIXING IN MYL2.5 MLM FOR SIMPLE WIND-MIXING CASE

MW97 used a simple, wind-mixing test case to look at the effects of LC on vertical mixing, and KC04 ran the same case to test their parameterization of LC mixing in the MYL2.5 MLM and to compare their results with those of MW97. Hence, we ran the same case to test our implementations of KC04's and H15's parameterizations of LC mixing in the version of the MYL2.5 MLM used in NCOM and to compare with the results of MW97 and KC04.

The initial condition for this test case consists of a SML with a depth of 33 m and a temperature of 13.5°C and a thermal stratification below the SML of 0.01°C/m. The salinity is set to a uniform 35 psu both within and below the SML. The initial temperature was chosen to give a thermal expansion coefficient of -0.0002 1/°C. The latitude is 43.4°N to give a value of the Coriolis parameter of 0.0001 1/s, which results in an inertial period of 17.45 h.

The forcing for the test case consists of a surface wind stress of 0.037 Pa, which corresponds to a wind speed of about 5 m/s. MW97 used a small cooling surface heat flux of 5 W/m^2 to speed up the convergence of their LES numerical solution and reduce its run time. We used a linear ramp the length of the inertial period (17.45 h) for the surface wind stress to reduce inertial oscillations and speed the convergence to an approximately steady solution.

The surface wave field for this test case was specified by MW97 as a monochromatic wave of amplitude 0.8 m and wavelength 60 m propagating in the downwind direction. This gives a SDC with a surface value of 0.0679 m/s and an e-folding depth (the inverse of twice the wavenumber, see Appendix A) of 4.78 m, which corresponds to a light swell.

NCOM was run for this case in what we refer to as pseudo one-dimensional mode by running the model on a horizontal domain of 2 by 2 grid points (the minimum horizontal grid that NCOM

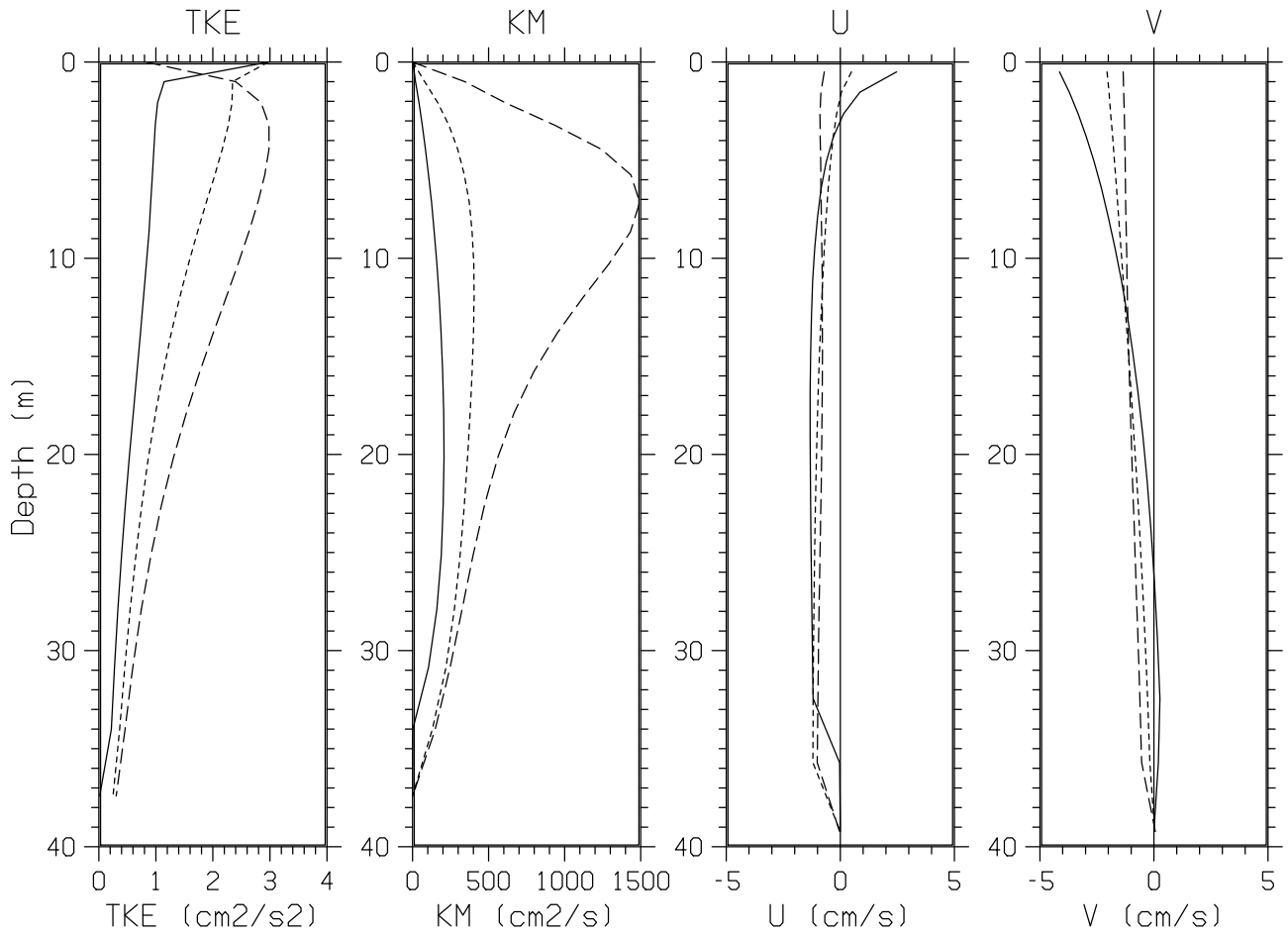

Fig. 2 — Profiles of TKE, vertical mixing rate for momentum, and downwind and crosswind velocity for simulations without a LCMP (solid line) and with the KC04 LCMP (dotted line) and H15 LCMP (dashed line) for the MW97, wind-mixing, test case.

allows) with doubly-periodic lateral boundary conditions. The vertical grid consisted of 40 layers with an upper-layer thickness of 1 m and a uniform stretching to a maximum depth of 200 m; hence, each layer is thicker than the layer above it by about 7%.

With the use of a linear ramp for the surface wind stress, the numerical solution is fairly steady once the ramp ends after 17.45 h. Figure 2 shows profiles of TKE, the vertical mixing coefficient for momentum, and the downwind and crosswind velocity for simulations without a LCMP and with the LCMPs of KC04 and H15. This figure can be compared with Fig. 2, 3, and 4 in MW97 and with Fig. 1 in KC04.

The TKE in Fig. 2 is roughly doubled by the use of the KC04 LCMP, which is qualitatively similar to the result in KC04. For the H15 LCMP, the TKE is roughly tripled, except for the reduction of the TKE for H15 in the upper 3 m. Note that the increase in TKE in the upper meter in Fig. 2 for the original MYL2.5 MLM and for the KC04 LCMP is due to the parameterization of the surface flux of TKE from the surface waves. The reduction of the TKE near the surface for the H15 LCMP is due to the effect of H15's surface proximity function.

For the KC04 LCMP, the maximum value of the vertical mixing coefficient for momentum K_M

in Fig. 2 is roughly doubled relative to the original MYL2.5 MLM, which is qualitatively similar to the result reported in KC04, i.e., the maximum value of K_M for the KC04 LCMP in Fig. 2 increases from about 200 to 400 cm^2/s, compared with an increase from about 215 to 430 cm^2/s in KC04 (their Fig. 1). For MW97 (their Fig. 3b), the maximum value of K_M increases by about a factor of 3 from about 130 to 380 cm^2/s. However, MW97's maximum value with the LC mixing (380 cm^2/s) is similar to that obtained in our simulation with the KC04 LCMP (400 cm^2/s) and by KC04 (430 cm^2/s). The shape of the original MYL2.5 and KC04 LCMP vertical mixing coefficient profiles in Fig. 2 is more similar to those in MW97 than in KC04 in that the profiles in Fig. 2 and in MW97 have a roughly parabolic shape, whereas the profiles in KC04 reduce fairly abruptly from a maximum value to a value close to zero within a short distance near the base of the SML.

For the H15 LCMP, the maximum value of K_M is about 1500 cm^2/s at 7 m depth. This is almost 4 times larger than the maximum value for the KC04 LCMP and about 7.5 times larger than the maximum value for the original MYL2.5 MLM. This large value of K_M for H15 is due to large values computed for H15's TKE (see Fig. 2) and stability functions, e.g., the value of S_M corresponding to the maximum value of K_M for H15 is about 1.15 compared with a value of 0.43 for KC04.

The component of the model's Eulerian velocity aligned with the wind u in Fig. 2 shows reduced shear with the stronger LC mixing and, as a result, the value of u at the surface is noticeably reduced, which is also shown in KC04 (their Fig. 1) and MW97 (their Fig. 2). The u profile for H15 in Fig. 2 shows less shear than for KC04 and the value at the surface is reduced as well to the point that it is upwind. Note that the velocity profiles in our Fig. 2, in Fig. 2 in MW97, and in Fig. 1 in KC04 are for just the models' Eulerian current and do not include the SDC.

With the inclusion of the SDC in the Coriolis term in the momentum equations, the net transport of u is not zero, but balances the net transport of the SDC u_s, so that the combined net downwind transport of the Eulerian current plus the SDC is zero. Hence, since the net transport of the SDC is downwind for this test problem, the net transport of the downwind component of the Eulerian current in the models is upwind as shown in Fig. 2 and by KC04 and MW97.

A difference in MW97 from the simulation here and in KC04 for the case without the LC mixing is that MW97 drop the SDC from the simulation completely, whereas here and in KC04 the SDC is retained in the calculation of the Coriolis term and is only turned off for the calculation of the vertical mixing in the MYL2.5 turbulence model. Hence, in Fig. 2 and in KC04's Fig. 1, the net transport of u for the case without LC mixing is still upwind to balance the net downwind transport of the SDC, whereas in MW97, the net transport of u for the case without LC mixing is zero (their Fig. 3).

The cross-wind velocity v in Fig. 2 also shows reduced shear with the LC mixing, similar to the cross-wind velocity in MW97 (their Fig. 2), and the surface value of the cross-wind velocity is, as a result, reduced. The reduction of the vertical shear and the surface value of the cross-wind velocity is greater for H15 than for KC04 because of H15's stronger mixing. The net transport of the cross-wind velocity must equal the Ekman transport for all of these simulations once they have reached near-equilibrium.

The profiles in Fig. 2 indicate slightly deeper mixing for the cases with the LCMP, i.e., for the case without the LCMP, the MLD increases from the initial value of 33 to 34 m, and for the cases

with the LCMP the MLD increases from 33 to about 37 m for both KC04 and H15. A deeper MLD with the LC mixing is also indicated in the results shown by MW97 and KC04.

The velocity profiles in KC04 (their Fig. 1) do not appear completely consistent, since the transports for the cases with and without LC mixing should be the same and they are somewhat different. This may be because the velocity profiles shown by KC04 have not reached equilibrium and there is some residual inertial motion present in the velocity profiles that they show.

In summary, the results obtained for the KC04 LCMP for this simple, wind-mixing test case are generally similar to the results reported in KC04 and MW97. The values of the maximum mixing rates for momentum are roughly doubled by including the LCMP in the results here and in KC04. This is less than the factor of three increase obtained by MW97, but the maximum mixing rate for momentum obtained here with KC04's LCMP of 400 cm^2/s is similar to that obtained by KC04 and MW97 with the LC mixing. The approximately parabolic shape of the eddy coefficient mixing profiles obtained here with NCOM are roughly similar to the shape of the eddy coefficient profiles obtained by MW97, but are somewhat different from the shape of the profiles in KC04.

For the H15 LCMP, the TKE is higher than for the KC04 LCMP, and the TKE decreases in the upper 3 m, whereas the TKE for the KC04 LCMP and the original MYL2.5 MLM increase near the surface due to the surface flux of TKE from the waves. The vertical mixing for H15 is much stronger than for KC04, i.e., the maximum value of K_M for H15 is 1500 cm^2/s vs 400 cm^2/s for KC04. The stronger mixing for the H15 LCMP results in less vertical shear in the wind-driven surface velocity profiles than for the KC04 LCMP.

4. TEST OF LC MIXING IN MYL2.5 MLM AT OWS PAPA

4.1 Description of Papa Simulations

OWS Papa was located in the northeast Pacific at about 145°W, 50°N from 1949 to 1981. The availability of long time series of meteorological and ocean subsurface measurements at Papa, and the fact that the effects of advection on the heat budget tend to be small in this area, have long made Papa a popular location to test and evaluate upper-ocean MLMs (Denman and Miyake 1973; Mellor and Durbin 1975; Martin 1985; Martin 1986; Gaspar 1988; Large et al. 1994; Kantha and Clayson 1994; Large 1996).

Simulations were conducted at OWS Papa for the year 1961 using NCOM run in pseudo one-dimensional mode and using the MYL2.5 turbulence model both with and without the LCMPs of KC04 and H15.

For the simulations at OWS Papa, a vertical grid of 100 layers was used, with a surface-layer thickness of 1 m and a smooth stretching to a maximum depth of 5500 m. Hence, each layer is thicker than the layer above by about 6%. This is higher vertical resolution than is typically used with NCOM. However, sensitivity tests have shown that the Mellor-Yamada-type mixing schemes in NCOM tend to predict a slighly deeper mixed layer and a smoother, better-resolved deepening of the mixed layer, as the vertical resolution is increased; this is especially noticeable at OWS Papa when the mixed layer deepens in the fall (Martin and Hogan, 2013). Hence, high vertical grid resolution was used for the Papa simulations to better illustrate the performance capabilities of the MLMs in comparisons with the observations at Papa.

Hourly surface wind stresses and heat fluxes were computed from the 3-hourly surface marine observations at Papa using fairly standard formulas as discussed in Martin (1985, 1986). Note that all the heat fluxes were pre-computed using the surface marine observations from Papa, i.e., the NCOM-predicted SST was not used in the calculation of any of the heat fluxes. The mean computed heat fluxes over the year were 105 W/m^2 for the solar radiation, -88 W/m^2 for the surface heat loss due to the net longwave and latent and sensible heat fluxes, and 18 W/m^2 for the net heat flux. These pre-computed heat fluxes are fairly consistent with the seasonal changes in the observed upper-ocean heat content at Papa during the spring and summer of 1961 (Martin et al. 2012), and this is the reason that all the heat fluxes are fixed and none (e.g., the latent and sensible heat fluxes) are computed using the model-predicted SST.

The solar extinction was taken to be Jerlov Type II (Jerlov 1968). The solar extinction (i.e., the depth of penetration of the solar radiation) can significantly affect the developement of the upper-ocean thermal structure in the summer (Martin, 1985), however, this effect tends to be larger at lower latitudes where the difference in the summer/winter heating is less pronounced and the winds and the deepening of the SML in the summer by the winds are reduced (Martin and Allard, 1993).

The ambient/background viscosity and diffusivity below the SML were taken to be 0.02 cm^2/s. The ambient diffusivity affects the predicted SST in the summer at Papa, since a larger value of the diffusivity causes a larger downward transport of heat out of the mixed layer and into the thermocline during the summer. The sharp seasonal thermocline that develops at Papa during the heating season suggests that the ambient diffusivity below the SML at this time is fairly small. The relative magnitudes of the ambient diffusivity and viscosity affect the deepening of the mixed layer, e.g., increasing the ambient viscosity relative to the ambient diffusivity tends to reduce the vertical shear of the horizontal velocity near the base of the SML and increase the local Richardson number and, hence, reduce the turbulent mixing (and visa versa).

A linear damping term in the momentum equations with a damping time scale of 10 d was used to provide some damping of the inertial oscillations, since the normal horizontal and vertical dissipation of these motions cannot be accounted for in one-dimensional simulations such as those being conducted here. Without such damping, inertial oscillations generated in the winter and spring when the SML is relatively deep can persist below the SML in the summer when the SML is shallow, and can affect the deepening of the SML in the fall when these persisting inertial oscillations are encountered by the deepening SML. Although interactions between a deepening SML and existing inertial oscillations commonly occur in the real ocean, inertial oscillations in the ocean are governed by three-dimensional processes that are not accounted for in a one-dimensional simulation, and it was considered best to avoid the artificial occurrance of encountering inertial oscillations generated and (unrealistically) left behind in the deeper water weeks or months earlier.

The initial condition for the simulations at Papa was a temperature profile from the bathythermograph (BT) observations at Papa for 1 January 1961, and a climatological salinity profile for the location of Papa for the beginning of January from the Levitus (1982) climatology. The salinity profiles at Papa feature a strong halocline between about 100 and 200 m that helps limit the depth of mixing in the winter.

Including the effect of the LCMPs of KC04 and H15 on the simulation of the SML at Papa requires an estimate of the SDC. Since we don't have wave observations for Papa for 1961, the SDC profile was estimated from the observed surface winds at Papa. As discussed in Martin et al.

(2013), there are a number of ways this can be done, e.g., (1) compute the SDC from the wind stress using empirical functions like those used by KC04 for their simulations at OWS Papa, (2) compute the SDC from the wind speed using wave energy spectra time-averaged for different wind speeds using wind and wave data from NOAA Buoy 46005 located in the northeast Pacific about 1100 km east-southeast of Papa, and (3) compute the SDC from the waves predicted by a wave model forced by the observed winds at Papa for 1961. Martin et al. (2013) found that these three methods for estimating waves at Papa resulted in, from (1) to (3), successively smaller wave effects. The method used in this report is (2), i.e., to estimate the waves from the wind based on relations between the wind and waves derived from observations from NOAA Buoy 46005. One reason for this choice is that this method includes swell, which always seems to be present in this area, even when the winds are light (Martin et al. 2012).

Nine years of wind and wave data from NOAA Buoy 46005 in the northeast Pacific were used to compute average wave spectra within 1-m/s-wide, wind-speed bins. These average wave spectra were then used to compute hourly SDC profiles at OWS Papa for 1961 based on the hourly wind speed at Papa. The details of this calculation can be found in Appendix B. Buoy 46005 is located at 131.001°W, 46.100°N, which is about 1100 km ESE of the location of OWS Papa. Hence, the wind and wave conditions in the area of the buoy should be roughly similar to those near OWS Papa. This calculation of the SDC at Papa will be referred to as the Buoy Wave Spectra (BWS) SDC.

4.2 Papa Simulations with MYL2.5 MLM without LC mixing

Figure 3 shows results from a simulation of the SML at Papa for 1961 using just the MYL2.5 MLM with no LCMP. However, note that the SDC is used in the Coriolis terms of the ocean model's momentum equations as discussed in Section 3. In the figure, the results of the simulation (red) are compared with the observations at Papa (black). The fields compared are SST, MLD, and isotherm depths (ISODs). The MLD shown in the figure is the depth at which the temperature becomes 0.2°C less than the SST. The isotherm depths are plotted at 1°C intervals and are temporally filtered to reduce the high-frequency variability and make them easier to discerne.

As in Martin (1985, 1986), the SST is too high in summer and, consistent with this, the MLD and ISODs are too shallow. In Fig. 3, the summer SST is about 2.5°C too high and the MLD and ISODs are 10 to 20 m too shallow in August and September. The agreement in Fig. 3 is a bit worse than in Martin (1985, 1986) because, for this simulation, the net surface heat flux has been set slightly higher to provide more net heating and better agreement with the observed upper-ocean heat content at Papa in the summer (Martin et al. 2012).

There are various methods of enhancing the depth of mixing obtained with the MYL2.5 MLM (Martin et al. 2013). KC94 used a parameterization of shear instability computed from the local Richardson number that was taken from Large et al. (1994, hereafter referred to as L94). The L94 shear-instability mixing parameterization (SIMP) provides a moderate level of mixing for Richardson numbers above the normal turbulence cutoff of 0.2–0.25 up to a Richardson number of 0.7. The maximum mixing rate for the L94 SIMP is 50 cm^2/s at a Richarson number of zero that decreases to zero at a Richardson number of 0.7. A more complete description of the L94 SIMP is provided in Appendix C.

KC94 described the parameterization as accounting for intermittent mixing due to reduction of

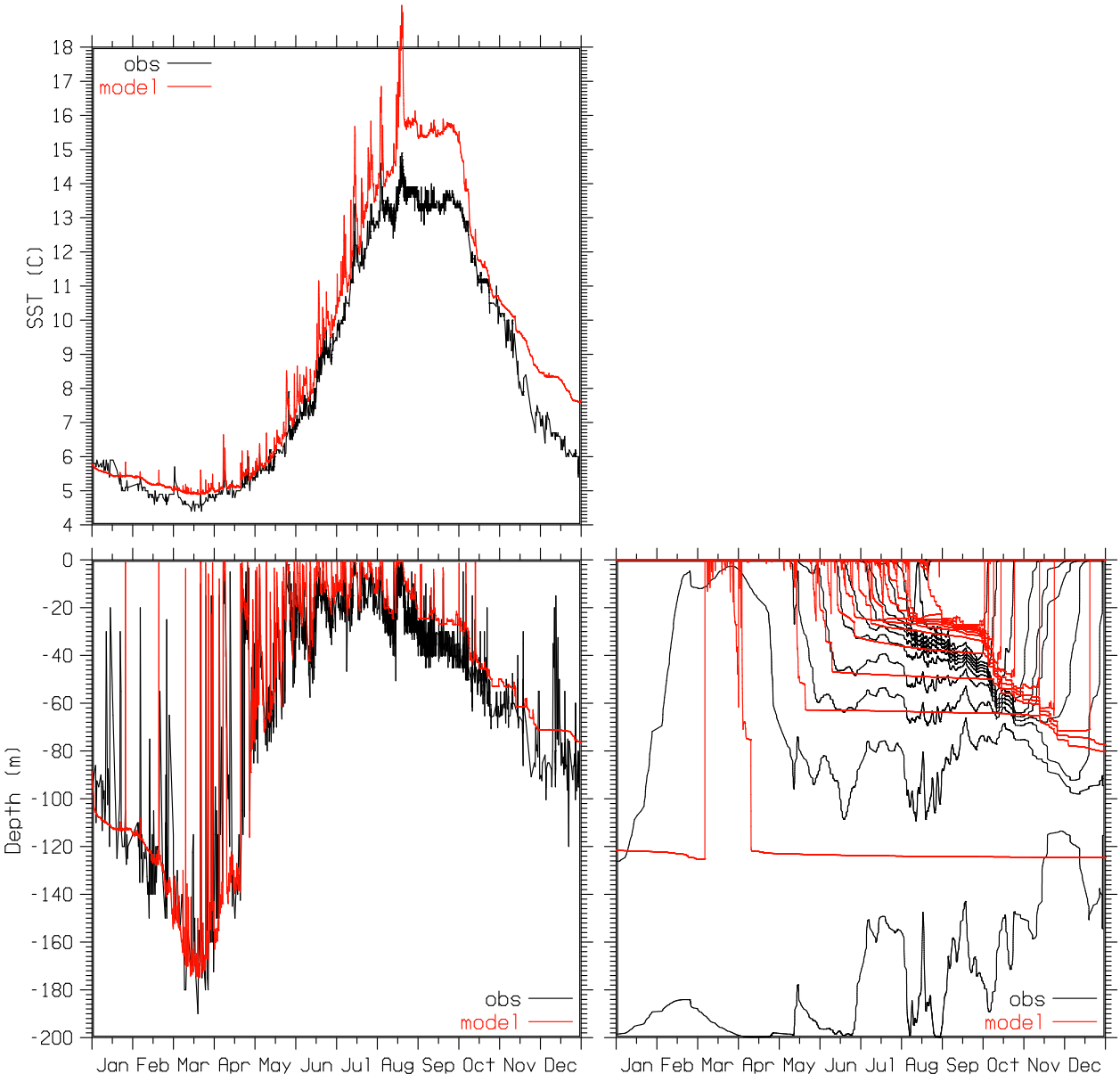

Fig. 3 — SST, MLD, and ISODs at OWS Papa for 1961: observed (black), simulated with the MYL2.5 MLM with no LCMP (red). ISODs are temporally filtered.

the local Ri by internal waves below the SML. L94 described this parameterization as accounting for shear instability due to resolved vertical shear below the SML (and they provided a separate parameterization for mixing by internal waves). Hence, L94 and KC94 do not seem to be in complete agreement as to what the L94 SIMP represents; however, its main effect is to provide some additional mixing for Richardson numbers above the normal critical value, which effectively increases the predicted depth of the SML. Both L94 and KC94 reported that the L94 SIMP improved agreement with observed MLDs for several open ocean data sets, including data from OWS Papa. Hence, the L94 SIMP may represent some unresolved or unaccounted for processes, including perhaps LC, that contribute to the deepening of the SML. The L94 SIMP has been available to enhance the vertical mixing of the Mellor-Yamada Level 2 turbulence model in NCOM, and NCOM was recently modified to allow the L94 SIMP to be used with the MYL2.5 turbulence model as well.

Figure 4 shows results from a simulation of the upper-ocean thermal structure at Papa using the MYL2.5 MLM with the L94 SIMP. With the L94 SIMP, the depth of the SML is significantly increased in the summer and fall and the MLD, ISODs, and SST all show better agreement with the observed values. That the SST and the MLD and ISODs simultaneously show fairly good agreement with the observations suggests that the net surface heat flux used for the simulation is a fairly good match for the actual changes in the upper-ocean heat content at Papa for 1961.

4.3 Papa Simulations with KC04 parameterization of LC mixing

Figure 5 shows results from a simulation of the upper-ocean thermal structure at Papa using the MYL2.5 MLM with the KC04 LCMP. Figure 5 shows that the simulation is slightly improved relative to that for the MYL2.5 MLM without the LCMP in Fig. 3, but the SST is still about 1.5°C too high in August and September and, consistent with this, the MLD and ISODs are too shallow. Hence, the use the KC04 LCMP slightly increases the predicted MLD, but the increase does not seem to be sufficient to account for the observed MLD at Papa in the summer.

Figure 6 shows results from a simulation of the upper-ocean thermal structure at Papa using the MYL2.5 MLM with both the KC04 LCMP and the L94 SIMP. As for the simulations with the MYL2.5 MLM in Fig. 3 and 4, the addition of the L94 SIMP significantly increases the MLD during the summer and fall. The MLD and ISODs at this time are now slightly too deep and, consistent with this, the SST is slightly too cool. Note that this simulation could be adjusted to better agree with the observations by reducing the value of the Richardson number at which the L94 SIMP cuts off mixing.

Figure 7 shows hourly values of the ratio of the maximum value of the vertical mixing coefficients K_M in the SML for the Papa simulations with and without the KC04 LCMP that are shown in Fig. 6 and 4, respectively (both these simulations use the L94 SIMP). Plots of the ratio of both unfiltered and temporally filtered K_M values are shown in Fig. 7.

The unfiltered plot shows that the range of the ratio of the K_M values is usually between about 0.5 and 3.5, with occasional lower and higher values. Values less than one indicate that the maximum value of K_M for the simulation with the KC04 LCMP is lower than that for the simulation without the LCMP.

The plot of the ratio of the temporally filtered K_M values shows a range between about 1 and 3

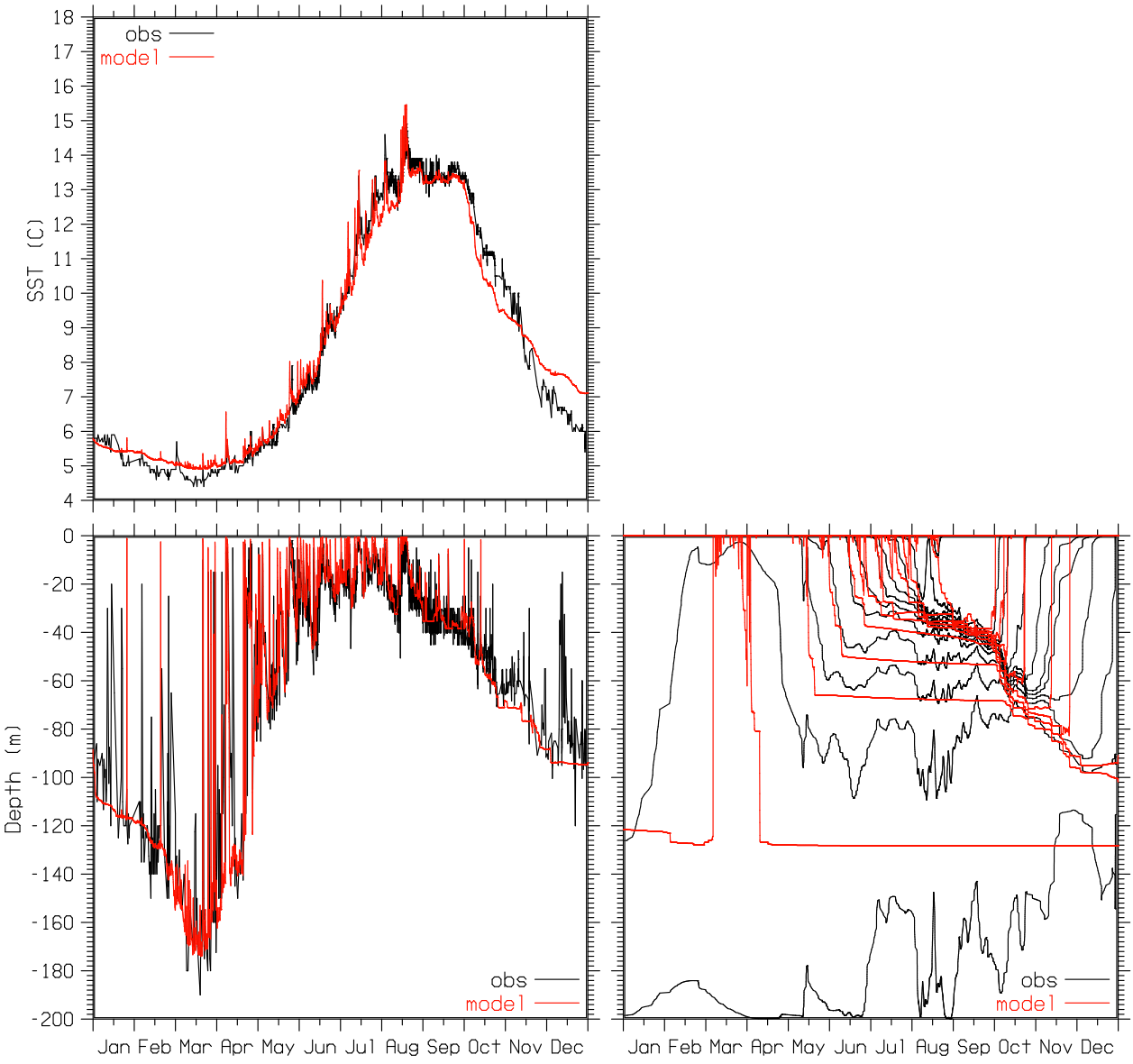

Fig. 4 — SST, MLD, and ISODs at OWS Papa for 1961: observed (black), simulated with the MYL2.5 MLM with the L94 SIMP (red). ISODs are temporally filtered.

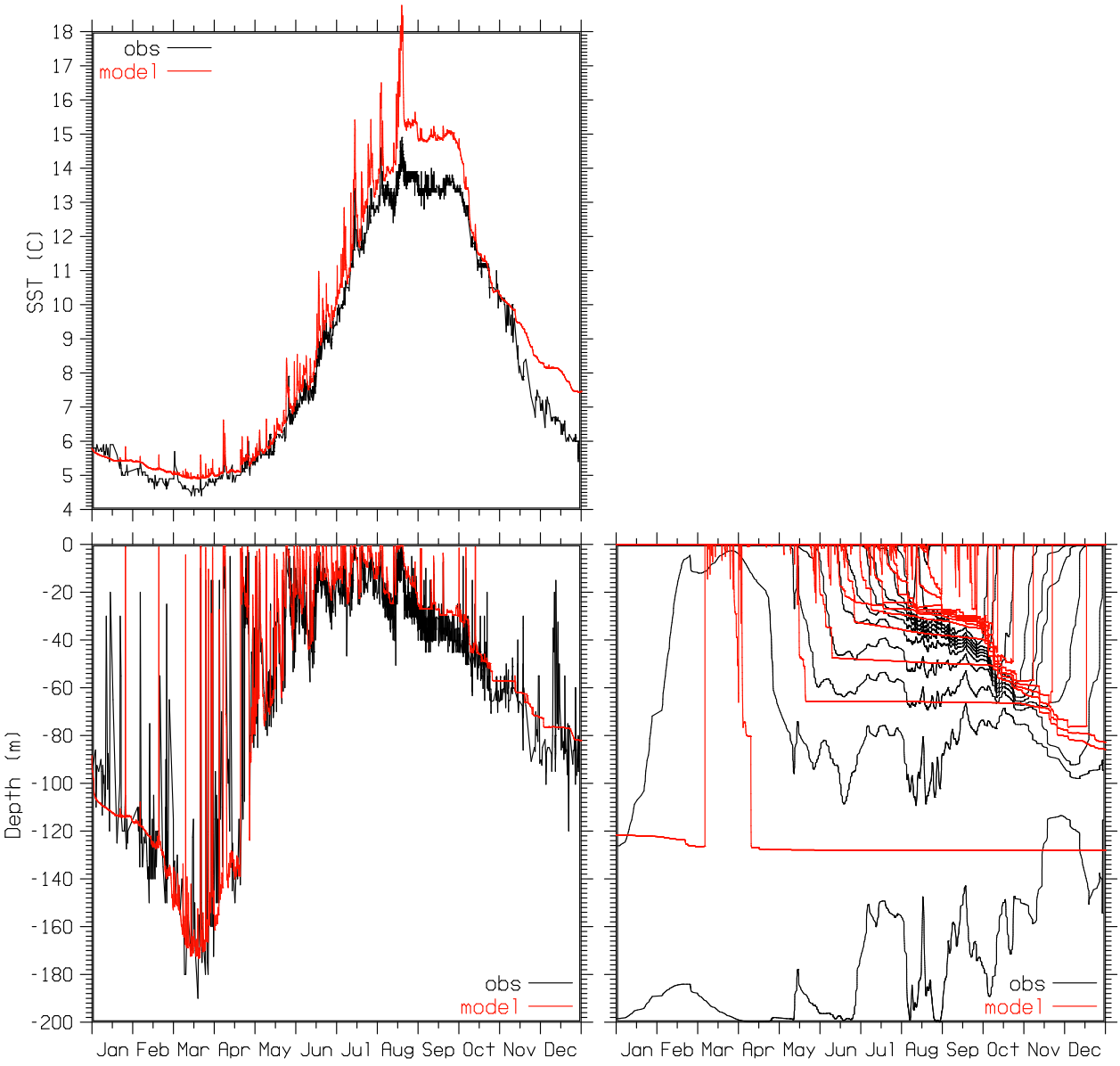

Fig. 5 — SST, MLD, and ISODs at OWS Papa for 1961: observed (black), simulated with the KC04 LCMP (red). ISODs are temporally filtered.

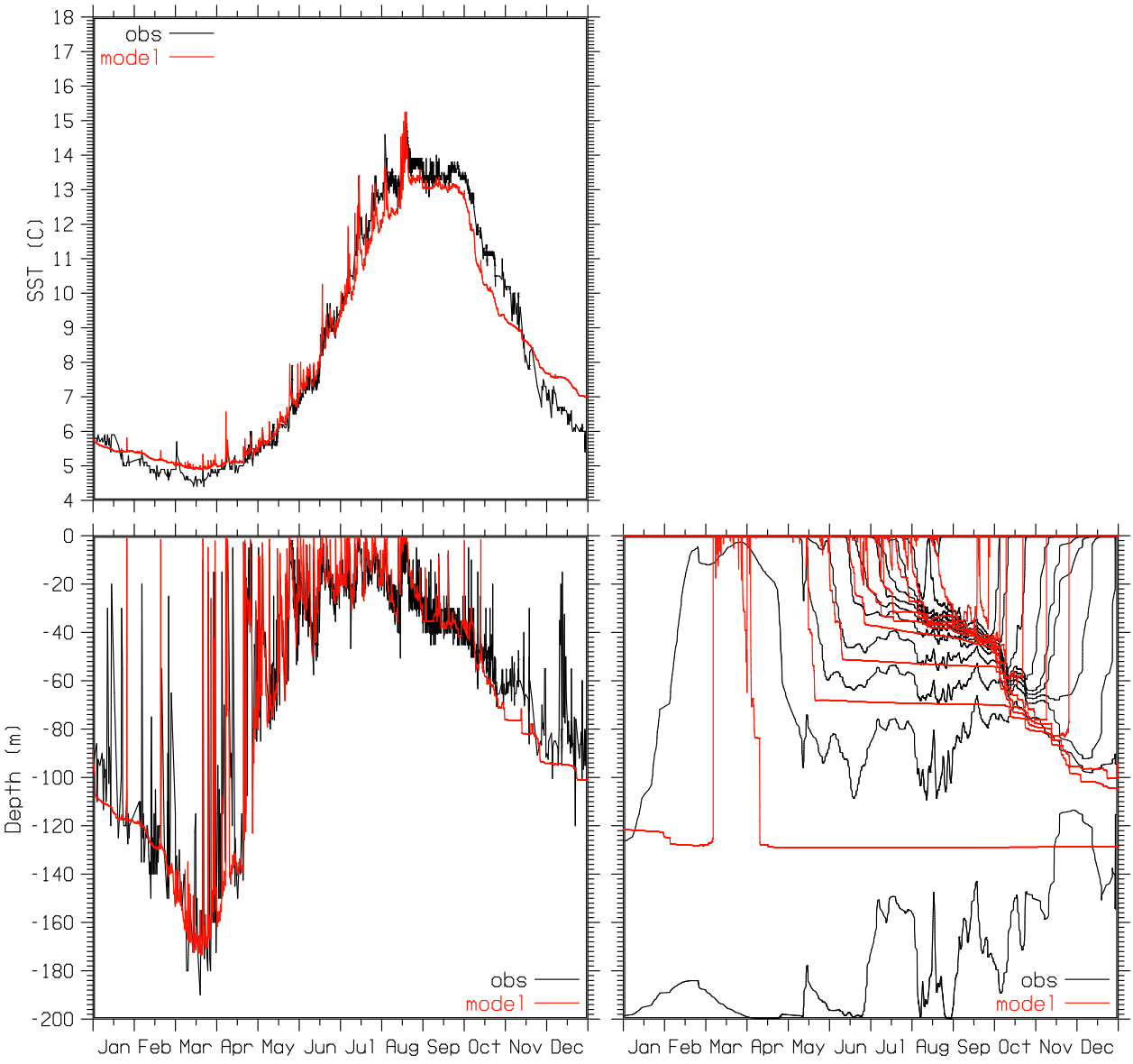

Fig. 6 — SST, MLD, and ISODs at OWS Papa for 1961: observed (black), simulated using both the KC04 LCMP and the L94 SIMP (red). ISODs are temporally filtered.

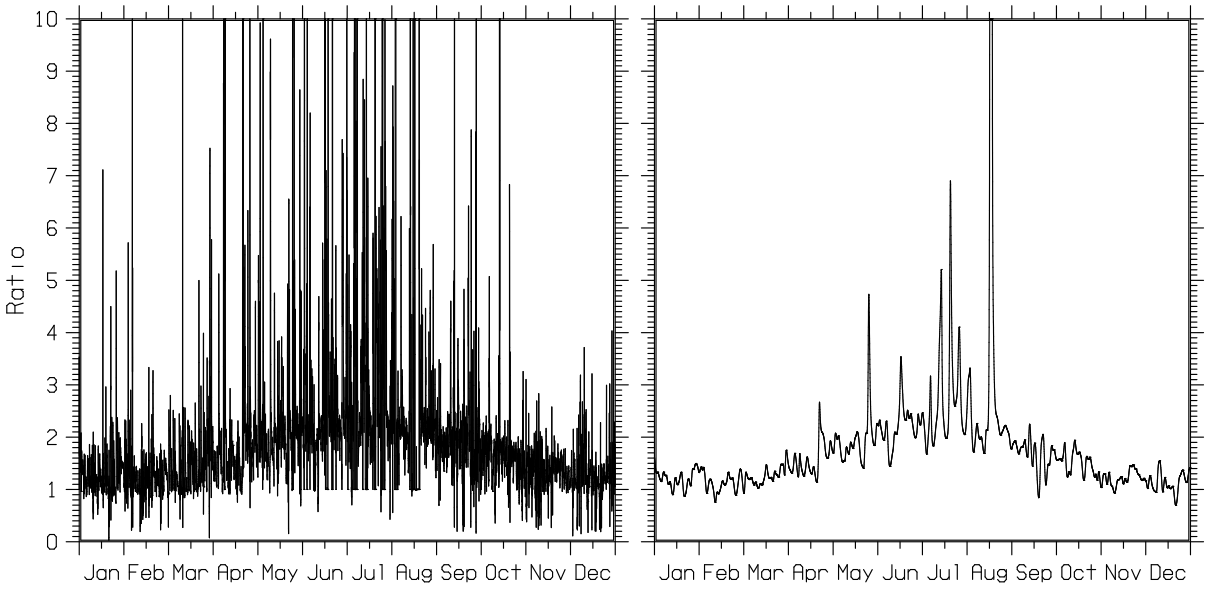

Fig. 7 — Hourly values of the ratio of the maximum value of the vertical mixing coefficients K_M in the SML for Papa simulations with and without the KC04 LCMP (both include the L94 SIMP). The left plot shows the ratio of unfiltered K_M values and the right plot shows the ratio of temporally filtered K_M values.

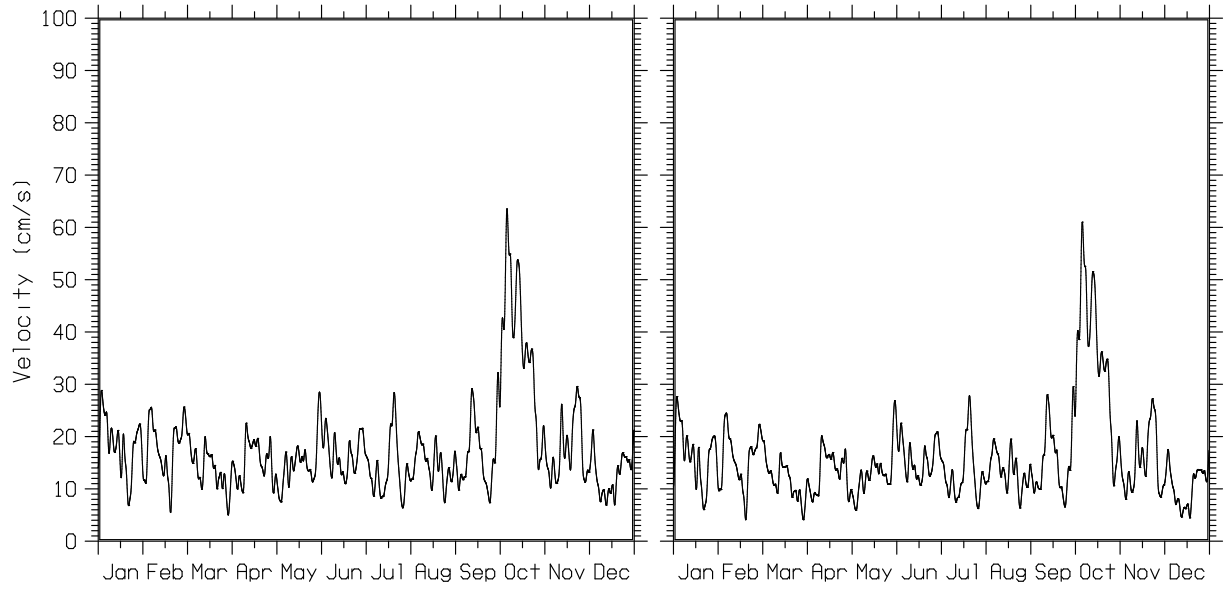

Fig. 8 — Surface current magnitude for simulation without the KC04 LCMP (left) and with the KC04 LCMP (right), both plots have had a strong temporal filter applied.

with occasional higher values. The ratio is smaller in the fall and winter when free convection, due mainly to surface cooling, plays a larger role in the vertical mixing, and is larger in the spring and summer when forced convection due to wind forcing and the resulting shear production of TKE plays a larger role. The mean value of the ratio in the spring and summer is about 2.3.

Figure 8 shows hourly values of the magnitude of the surface current for the Papa simulations without and with the KCO4 LCMP (note that these time series have been temporally filtered). The mean value of the magnitude of the surface current is reduced about 10% over the year when the KC04 LCMP is used. This is somewhat less than the reduction of the surface current by the KC04 LCMP shown in Fig. 2. This is partly because of the frequent occurrence of inertial oscillations in the Papa simulations, which tend to be fairly uniform with depth in the SML and

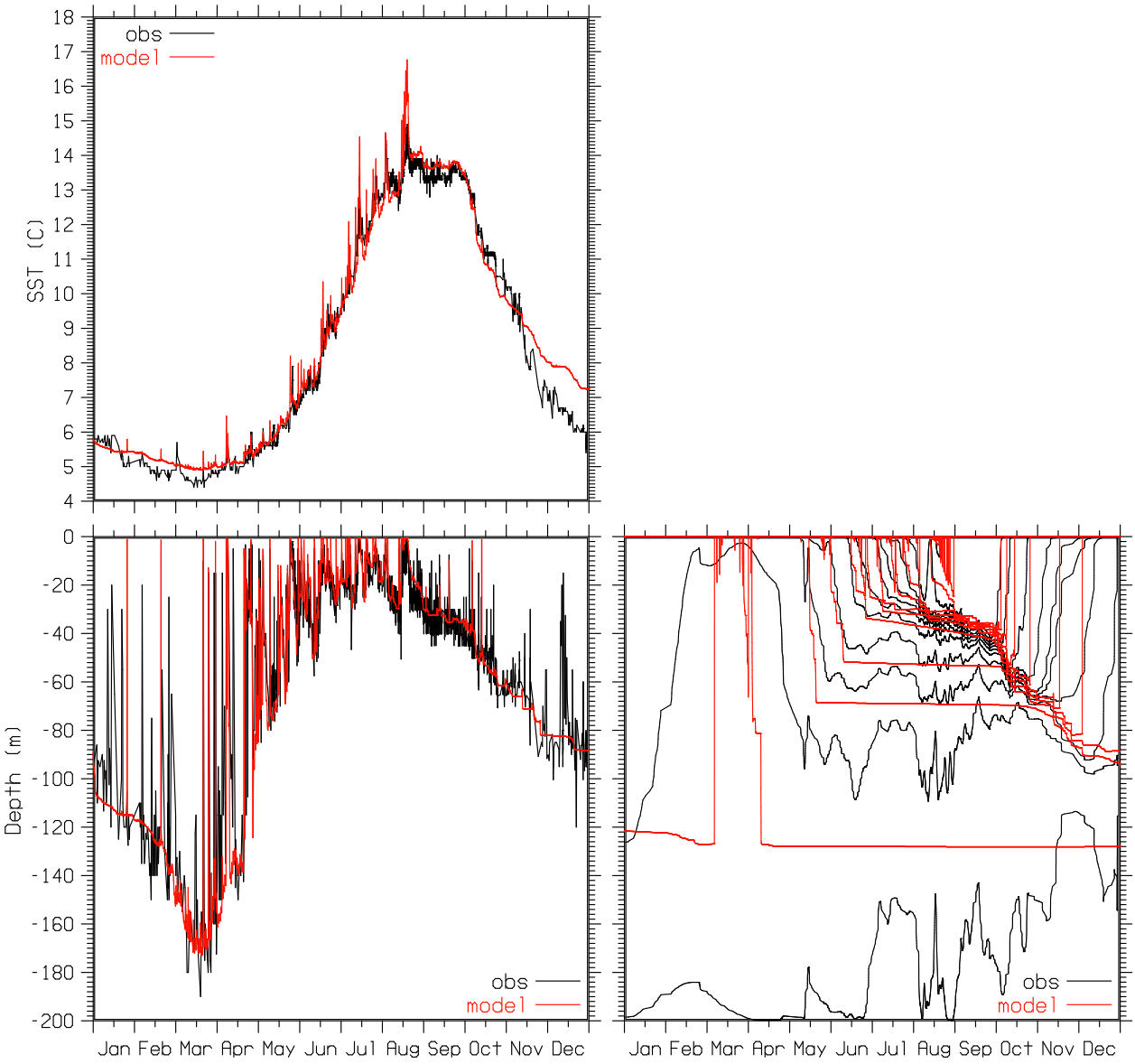

Fig. 9 — SST, MLD, and ISODs at OWS Papa for 1961: observed (black), simulated with the H15 LCMP (red). ISODs are temporally filtered.

are not significantly affected by the strength of the vertical mixing, whereas for the velocity profiles in Fig. 2 the inertial oscillations were suppressed by turning on the wind forcing gradually using a linear ramp over one inertial period.

4.4 Papa Simulations with H15 parameterization of LC mixing

Figure 9 shows results from a simulation of the upper-ocean thermal structure at Papa using the MYL2.5 MLM with the H15 LCMP. Note that this simulation is not using the L94 SIMP. Comparison of this simulation with the earlier Papa simulations indicates that the H15 LCMP predicts an overall deeper SML than the original MYL2.5 MLM and the KC04 LCMP (Fig. 3 and 5, respectively), and provides a good simulation of the SST, MLD, and ISODs at Papa without

much need for additional mixing enhancements. The SST is slightly too warm in summer and the MLD and IDODs are, correspondingly, slightly too shallow.

Since the H15 LCMP has shear-production terms in the TKE and TLS equations (19-20) that depend only on the shear produced by the SDC, there was some concern whether the H15 LCMP would predict adequate shallowing during light-wind conditions at Papa, since some swell is always present. However, Fig. 9 indicates that the H15 LCMP predicts shallowing and SST peaks during calm wind conditions similar to the original MYL2.5 MLM and the KC04 LCMP.

Figure 10 shows hourly values of the ratio of the maximum value of the vertical mixing coefficients K_M in the SML for the H15 and KC04 Papa simulations shown in Fig. 9 and 6, respectively (the KC04 simulation here uses the L94 SIMP but the H15 simulation does not). Plots of the ratio of both unfiltered and temporally filtered K_M values are shown. The unfiltered K_M ratios show a large range. The filtered K_M ratios show values between about 1 and 5, with a mean value in the spring and summer of 2.8. Hence, as in the simple mixing test case (Fig. 2), the H15 LCMP predicts significantly higher mixing rates for the shear-generated TKE than the KC04 LCMP. A plot of the time-filtered surface current magnitudes for these two simulations (not shown) indicates that the mean surface currents are similar.

Li et al. (2005) describe a regime diagram for classifying turbulent mixing in the upper ocean. Such a diagram is presented here in Fig. 11 for OWS Papa for 1961 using the SDC estimated from the wind and wave data from NOAA Buoy 46005 (i.e., the BWS). The figure shows a scatter plot of hourly values of the Hoenikker number versus the turbulent Langmuir number for Papa for 1961. The Hoenikker number H_o is given by

$$H_o = \frac{4B_0 d_s}{V_s(0) u_*}, \tag{37}$$

where B_0 is the total surface buoyancy flux, d_s is the e-folding depth of the SDC, $V_s(0)$ is the surface value of the SDC, and u_* is the water-side surface friction velocity. The turbulent Langmuir number La_t is given by

$$La_t = (\frac{u_*}{V_s(0)})^{1/2}. \tag{38}$$

The diagram is divided into three regimes according to the type of turbulent mixing: Langmuir, convection, or shear, that dominates within that region. The boundaries of the three regimes were determined by Li et al. (2005) based on LES experiments. The regimes are characterized by the relative magnitudes of the components of the turbulent mixing, with the vertical component dominating in convective mixing, the downwind component dominating in shear mixing, and the cross-wind and vertical components dominating the downwind component in Langmuir mixing.

Figure 11 indicates that the upper-ocean mixing at Papa for 1961 is generally in the Langmuir and convection regimes. Only a few points occur in the shear regime, and these occur close to the boundary between the shear and Langmuir regimes. This is consistent with the finding of Li et al. (2005) that wind mixing in the upper-ocean typically occurs in the Langmuir regime.

As noted in Section 2.3, the behavior of the H15 turbulence parameterization when the SDC is zero is of interest, since the SDC in the SML will be small when the waves are small, and will be

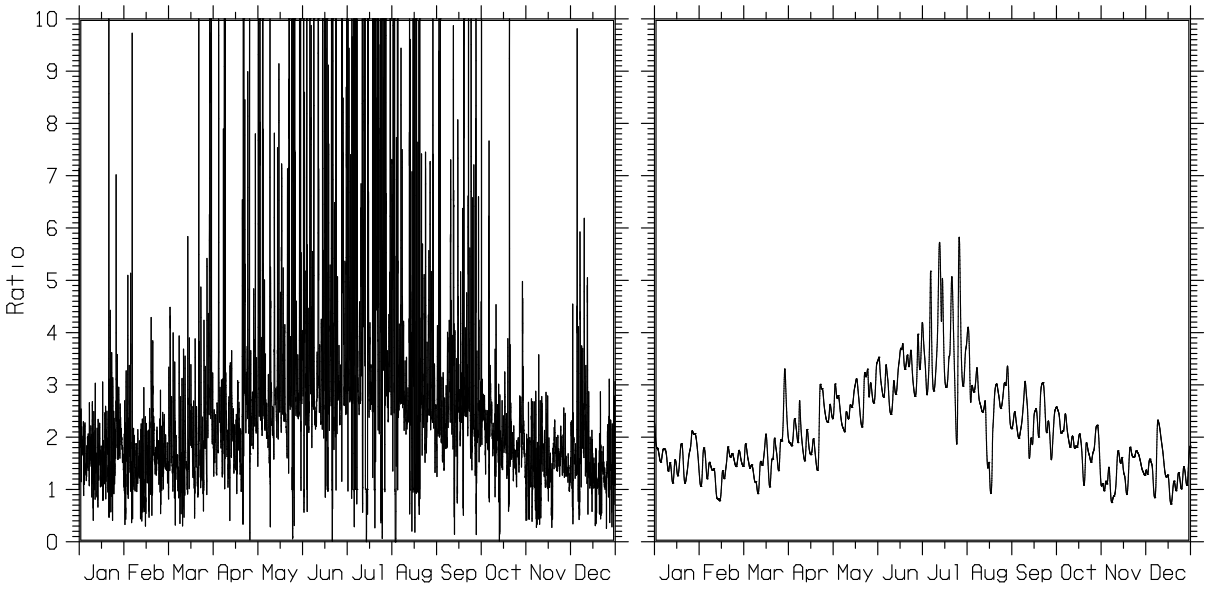

Fig. 10 — Hourly values of the ratio of the maximum value of the vertical mixing coefficients K_M in the SML for Papa simulations with the H15 LCMP and with the KC04 LCMP. The left plot shows the ratio of unfiltered K_M values and the right plot shows the ratio of temporally filtered K_M values.

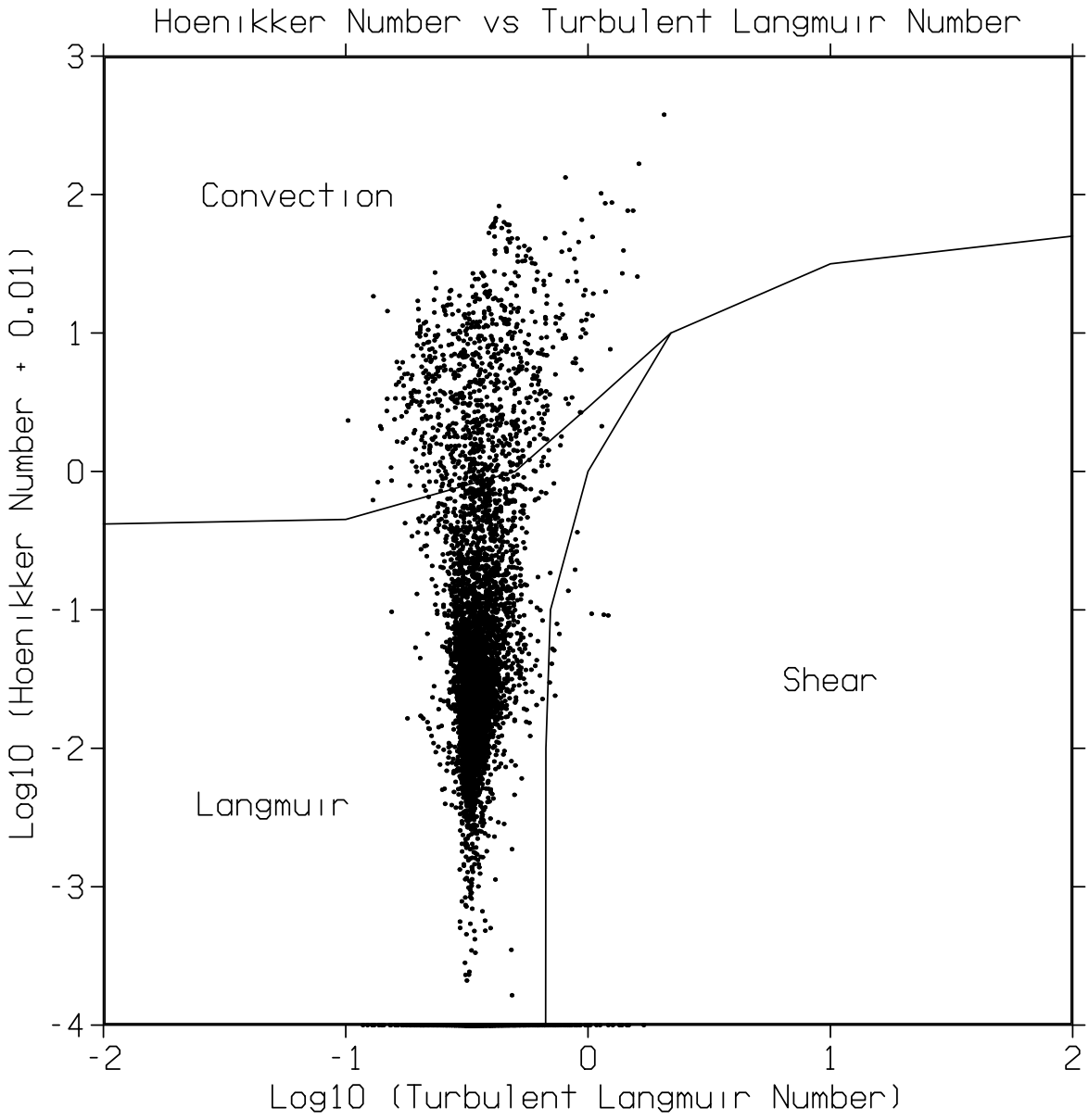

Fig. 11 — Turbulent regime diagram for OWS Papa for 1961 using the SDC computed from the BWS. The points plotted are hourly values of the log10 of the Hoenikker number (with an offset of 0.01) versus the log10 of the turbulent Langmuir number.

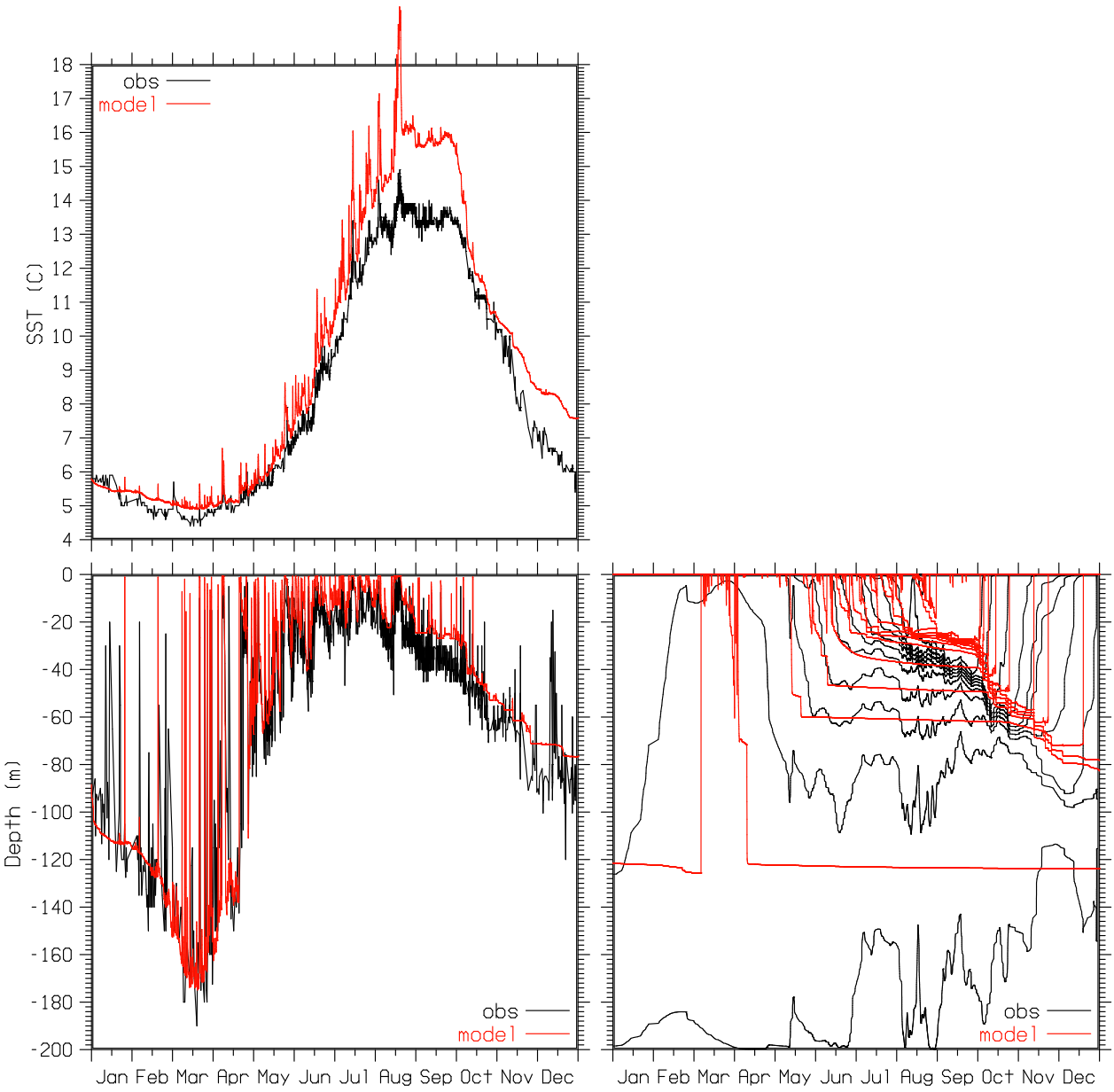

Fig. 12 — SST, MLD, and ISODs at OWS Papa for 1961: observed (black), simulated with the H15 LCMP with SDC=0 (red). ISODs are temporally filtered.

zero in deep mixed layers below the influence of the surface waves. Figure 12 shows results from a simulation at Papa with H15 with the SDC set equal to zero. The MLD is shallower than in Fig. 9 for H15 with the SDC, and is similar to the MLD for the MYL2.5 turbulence model without LCMP mixing in Fig. 3.

5. TEST OF LC MIXING IN MYL2.5 MLM FOR HURRICANE IVAN SIMULATIONS

Simulations were run with NCOM in the Gulf of Mexico (GoM) with wave forcing from SWAN to look at the effect of the KC04 and H15 LCMPs on a simulation of the response of the ocean in the GoM to Hurricane Ivan in September 2004. Atmospheric forcing was provided from a

simulation of Hurricane Ivan with the COAMPS atmospheric model. COAMPS, which stands for Coupled Ocean/Atmosphere Mesoscale Prediction System (Chen et al. 2010), is currently a coupled atmosphere-ocean-wave modeling system. However, for the simulations conducted here, the atmosphere, ocean, and wave models were run separately. Within the rest of this report, COAMPS will be used to refer to just the COAMPS atmospheric model (Hodur 1997).

NCOM was run with a horizontal grid resolution of about 4 km. NCOM's vertical grid consisted of 40 layers with a surface layer thickness of 1 m and a smooth stretching to a maximum depth of 5500 m. Initial and boundary conditions for NCOM were provided by the Global NCOM model that is run operationally at the Naval Oceanographic Office at Stennis Space Center, Mississippi (Barron et al. 2004). The COAMPS atmospheric model was run as a triply-nested system with grid resolutions of 81, 27, and 9 km. Initial and boundary conditions for COAMPS were provided by the Navy Operational Global Atmospheric Prediction System (NOGAPS), which was run at the Navy's Fleet Numerical Meteorology and Oceanography Center (FNMOC) in Monterey, California (Rosmond et al. 2002). Hourly surface fields from COAMPS's innermost grid were used to force SWAN and NCOM. These fields include the surface winds for SWAN, and the surface wind stress, surface pressure, solar radiation, net longwave radiation, latent and sensible heat fluxes, evaporation, and precipitation for NCOM. SWAN was run on the same 4-km horizontal grid as NCOM.

Wave fields for forcing NCOM were output hourly from SWAN and include the surface wave radiation stress, the SDC profiles, and the characteristic amplitude, frequency, and direction of the orbital wave motion near the ocean bottom. The wave radiation stress forcing in NCOM is implemented similar to the surface wind stress as a surface stress. In the open sea, the wave radiation stress forcing of the ocean is relatively small, i.e., generally less than 10% of the magnitude of the wind stress. The SDC, as noted in Section 2, is used in NCOM's Coriolis and advection terms, in the continuity equation, and also in the KC04 and H15 LCMPs. The wave orbital motions near the bottom act to enhance the ocean model's bottom drag in areas where the bottom is sufficiently shallow to feel the orbital wave motions (Grant and Masden 1979; Soulsby 1995). However, the focus here is only on the effect of the KC04 and H15 LCMPs; hence, the NCOM simulations that are compared all have full wave forcing from SWAN, and the only difference between them is whether the LCMPs of KC04 or H15 are used or not.

The ocean model simulation was started at 00Z on 12 September 2004, at which time Hurricane Ivan was in the central Caribbean Sea. Figure 13 shows the SST and sea-surface velocity (SSV) vectors for the simulation with the H15 LCMP for 09Z 15 September. Hurricane Ivan is near the center of the GoM at this time. The surface wind vectors from the COAMPS atmospheric model are also shown in the plot. Note that the surface current vectors in Fig. 13 include both the NCOM surface current and the SDC from SWAN. The hurricane winds generate strong cooling along the hurricane track, with the strongest cooling usually occurring just to the right of the track (Price 1981). The equivalent plot for the simulation with the KC04 LCMP looks very similar (this plot is shown in M13 in Fig. 14, but is not shown here).

Figure 14 shows the difference in the SST between the simulation with the H15 LCMP (Fig. 13) and with no LCMP (not shown) at 09Z 15 September 2004. The simulation with the H15 LCMP generally shows more cooling of the SST near the hurricane, as indicated by the areas of negative temperature difference; the difference is typically a few tenths of a °C and the maximum difference

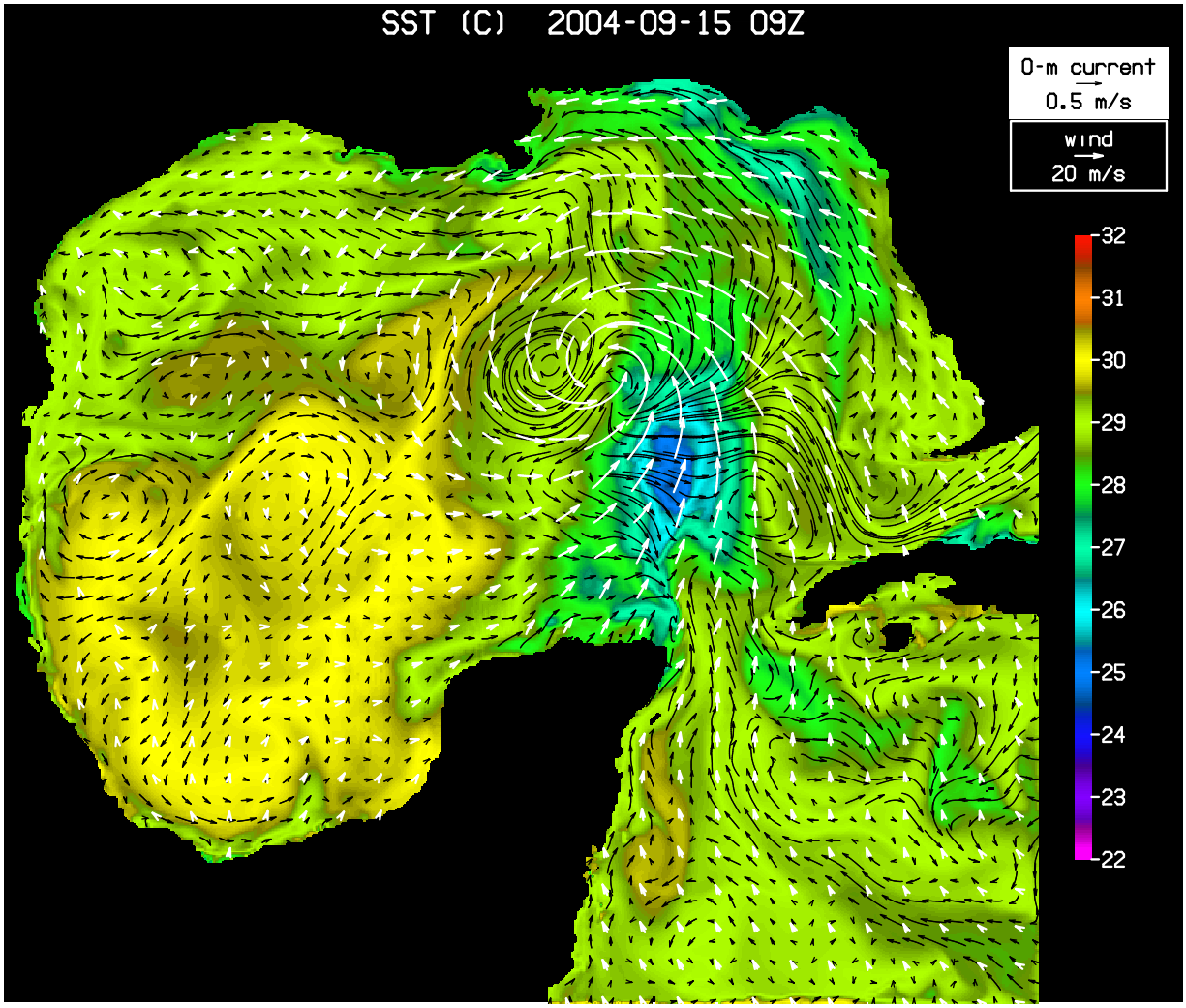

Fig. 13 — SST (color contours), SSV (black vectors), and surface winds (white vectors) at 09Z 15 September 2004 for simulation of Hurricane Ivan with the H15 LCMP

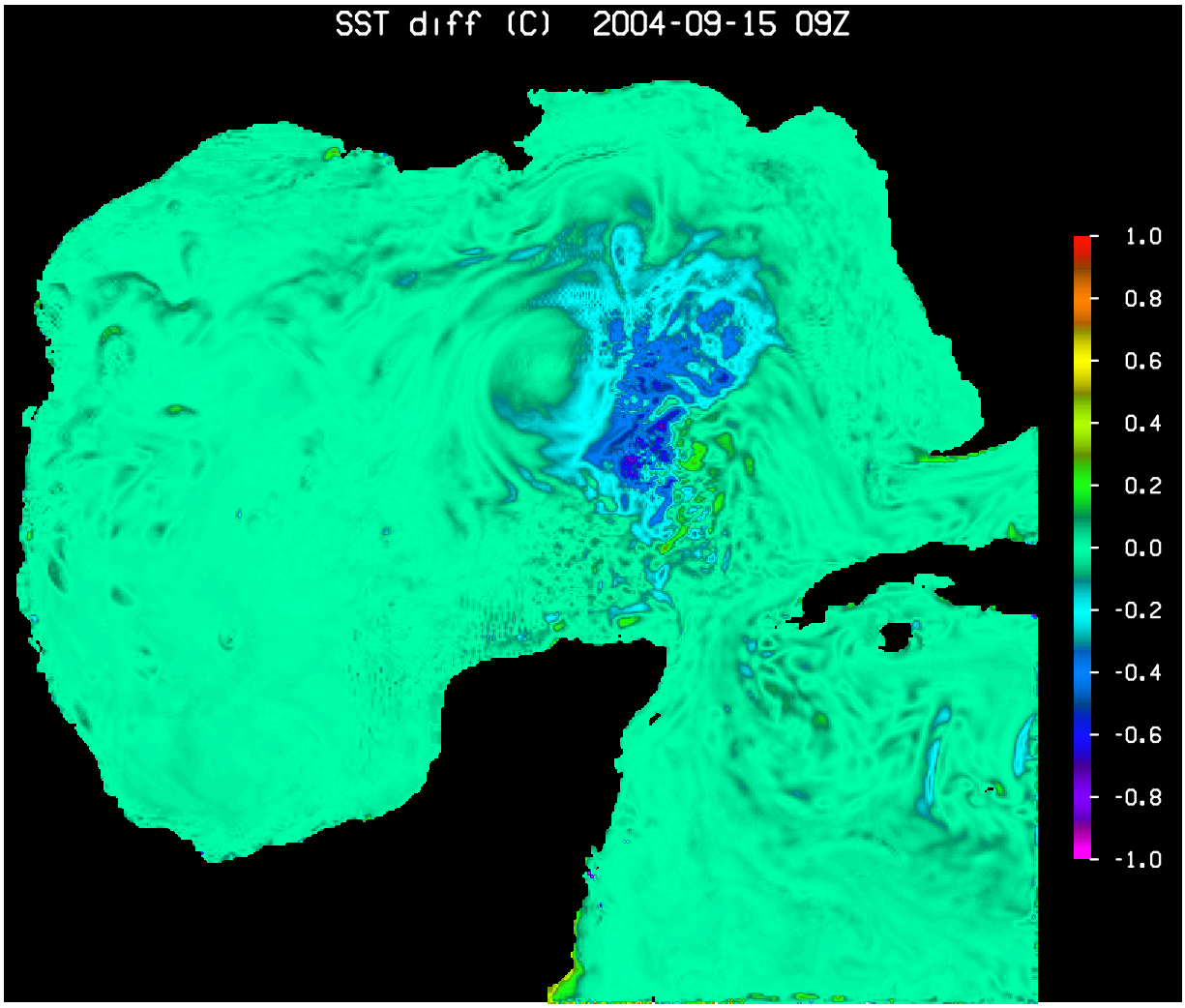

Fig. 14 — Difference in SST for Hurricane Ivan simulations with the H15 LCMP and without a LCMP at 09Z 15 September 2004.

is about 0.8°C. The lower SST for the simulation with the H15 LCMP indicates deeper mixing, which is consistent with the results at OWS Papa in Section 4.

Figure 15 shows the equivalent plot to Fig. 14 for the KC04 LCMP (note, however, that the temperature range in Fig. 15 is half that used for Fig. 14). The additional cooling for the KC04 LCMP compared to the original MYL2.5 MLM without an LCMP is generally small, i.e., less than 0.5 °C, and is significantly less than that in Fig. 14, which is consistent with the results at OWS Papa.

Figure 16 shows the difference in the SSV between the simulation with the H15 LCMP and without at 09Z 15 September 2004. The color contours show the difference in the magnitude of

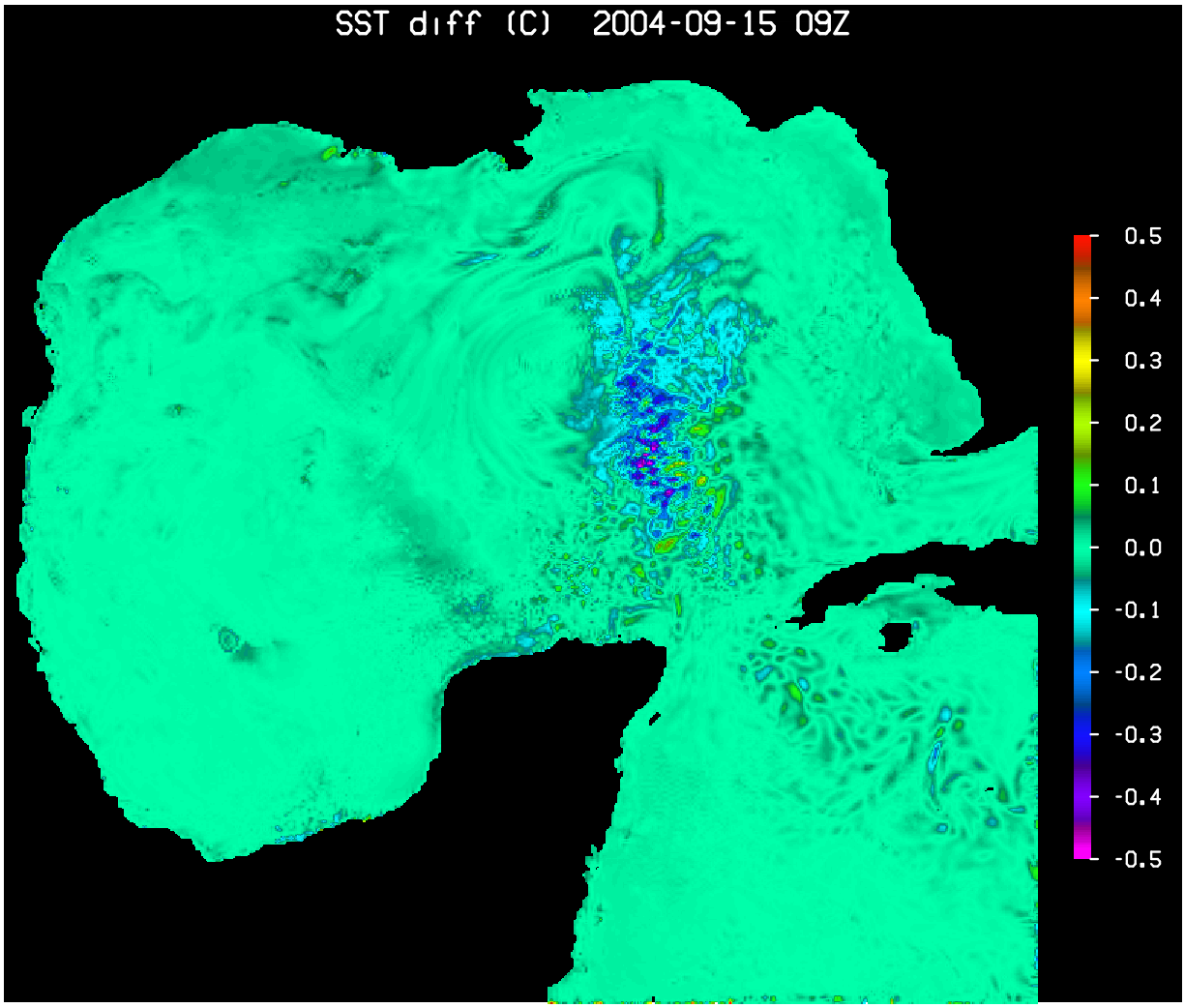

Fig. 15 — Difference in SST for Hurricane Ivan simulations with KC04 LCMP and with no LCMP at 09Z 15 September 2004.

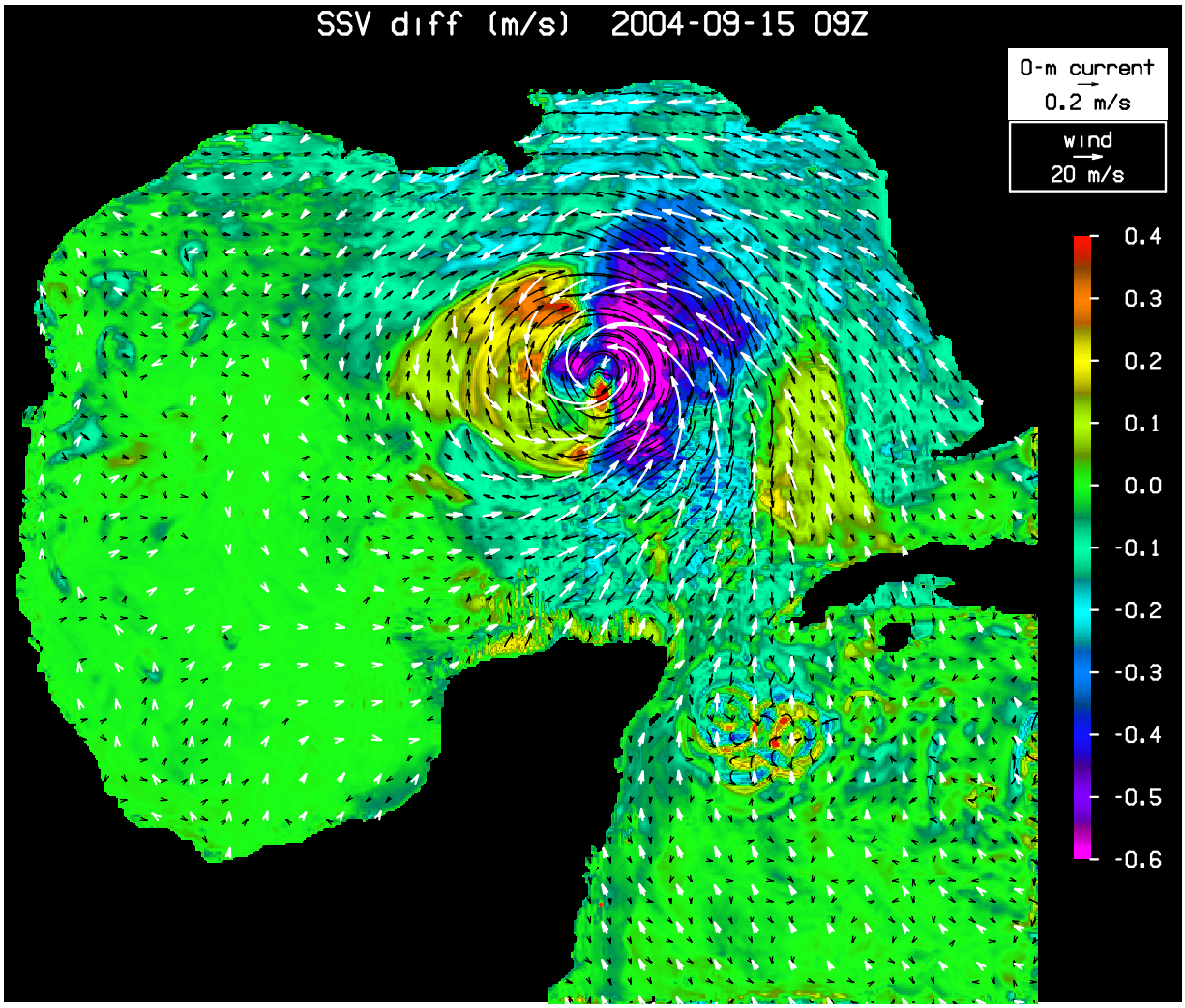

Fig. 16 — Difference in SSV for Hurricane Ivan simulations with the H15 LCMP and for the original MYL2.5 MLM without a LCMP at 09Z 15 September 2004. The color contours show the difference in the magnitude of the surface current and the black vectors show the vector velocity difference. The white vectors show the surface winds.

the surface current and the black vectors show the vector velocity difference. The fact that the direction of the velocity difference vectors is opposite to the wind direction indicates that the stronger mixing with the H15 LCMP reduces the wind-driven surface currents. Near the hurricane, the surface currents are reduced by 30–50 cm/s or more. Some areas show the surface current magnitude with the H15 LCMP to be larger (as indicated by the color contours in Fig. 16) and this is because the direction of the prevailing currents in these areas is nearly opposite to the wind direction, and so a reduction in the downwind, wind-driven current increases the total current, e.g., on the west side of the hurricane there is an anti-cylonic Loop Current eddy (see Fig. 13).

The reduction of the surface current for the KC04 LCMP (Fig. 17) is less than for the H15 LCMP (Fig. 16), since the vertical mixing rates are not as strong.

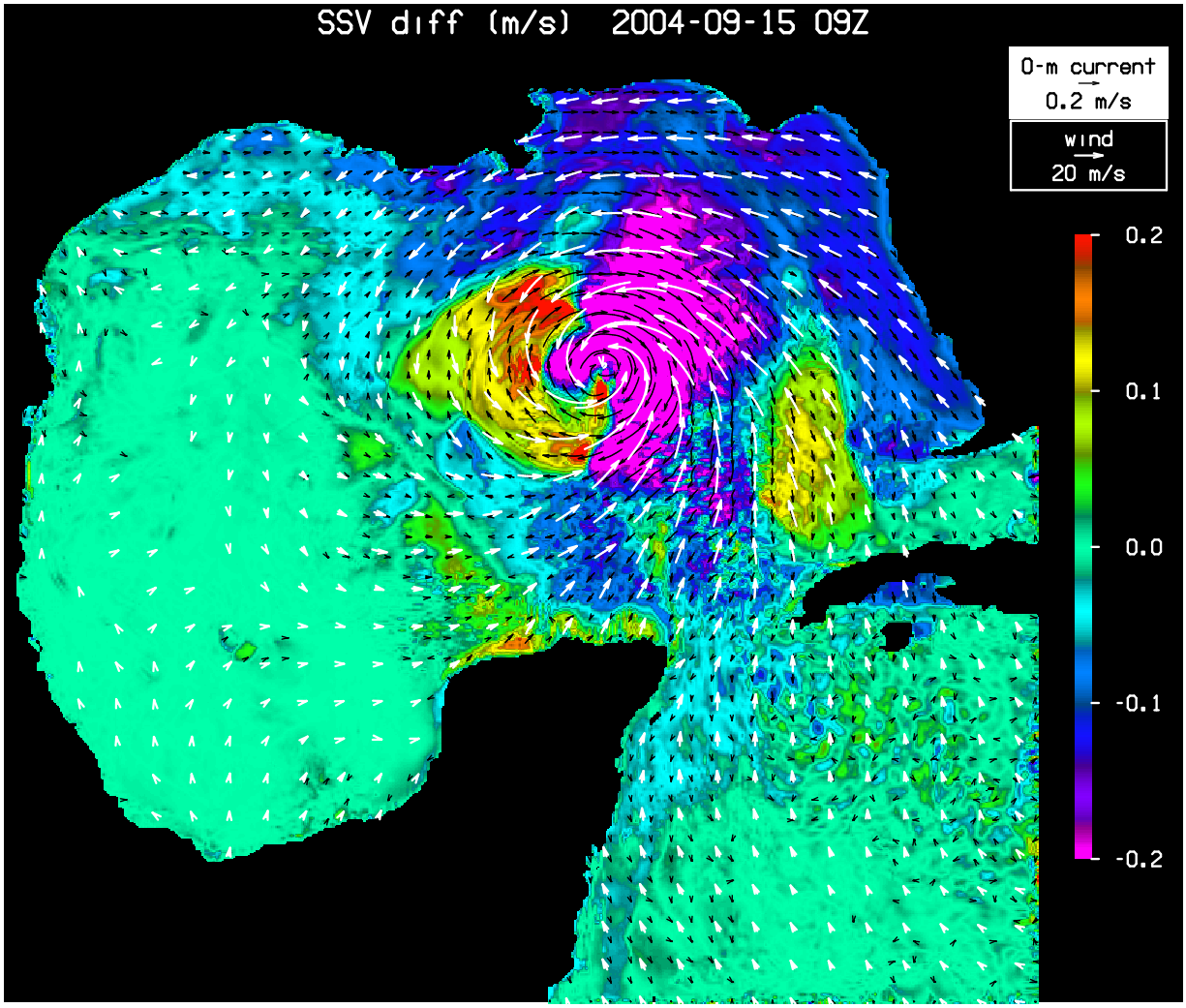

Fig. 17 — Difference in SSV for Hurricane Ivan simulations with the KC04 LCMP and without a LCMP at 09Z 15 September 2004. The color contours show the difference in the magnitude of the surface current and the black vectors show the vector velocity difference. The white vectors show the surface winds.

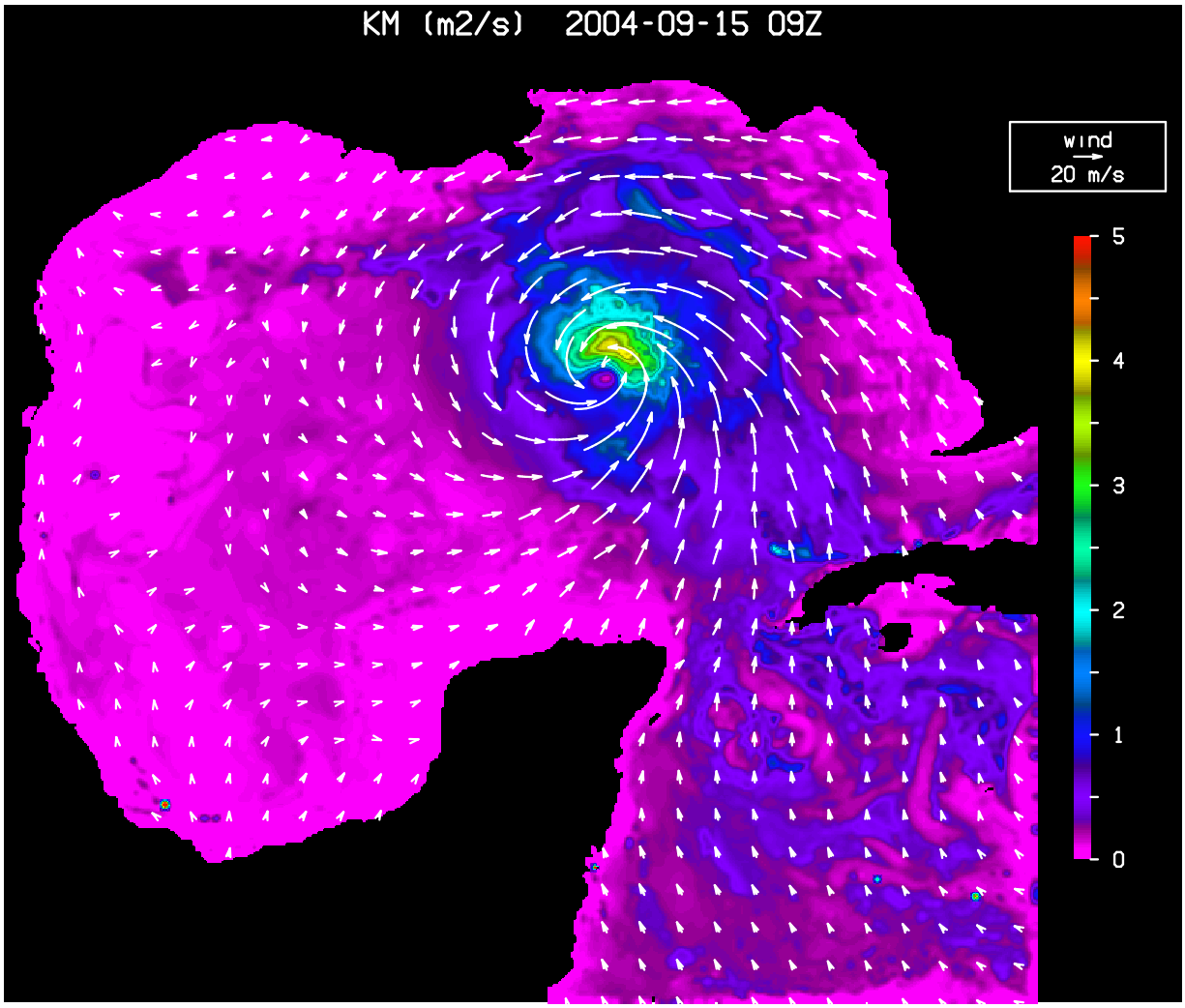

Fig. 18 — Maximum value of K_M in SML for Hurricane Ivan simulation with H15 LCMP at 09Z 15 September 2004. The white vectors show the surface winds.

Figure 18 shows the maximum value of the vertical mixing coefficient K_M in the SML for the simulation with the H15 LCMP at 09Z 15 September 2004. The K_M values in Fig. 18 were spatially filtered with one pass of a 3x3 box filter. The strongest mixing near the hurricane is occurring on the northeast side of the eye, with maximum values of K_M of 4 m^2/s. A circular area of weak mixing occurs under the eye of the hurricane due to the lighter winds there.

Figure 19 shows the maximum value of the vertical mixing coefficient K_M in the SML for the simulation with the KC04 LCMP at 09Z 15 September 2004. The K_M values in Fig. 19 were also spatially filtered with one pass of a 3x3 box filter. The strongest mixing near the hurricane is occurring on the north and east sides of the eye, with maximum values of K_M of about 1 m^2/s.

The local time for Fig. 19 is about three o'clock in the morning; hence, there is relatively strong

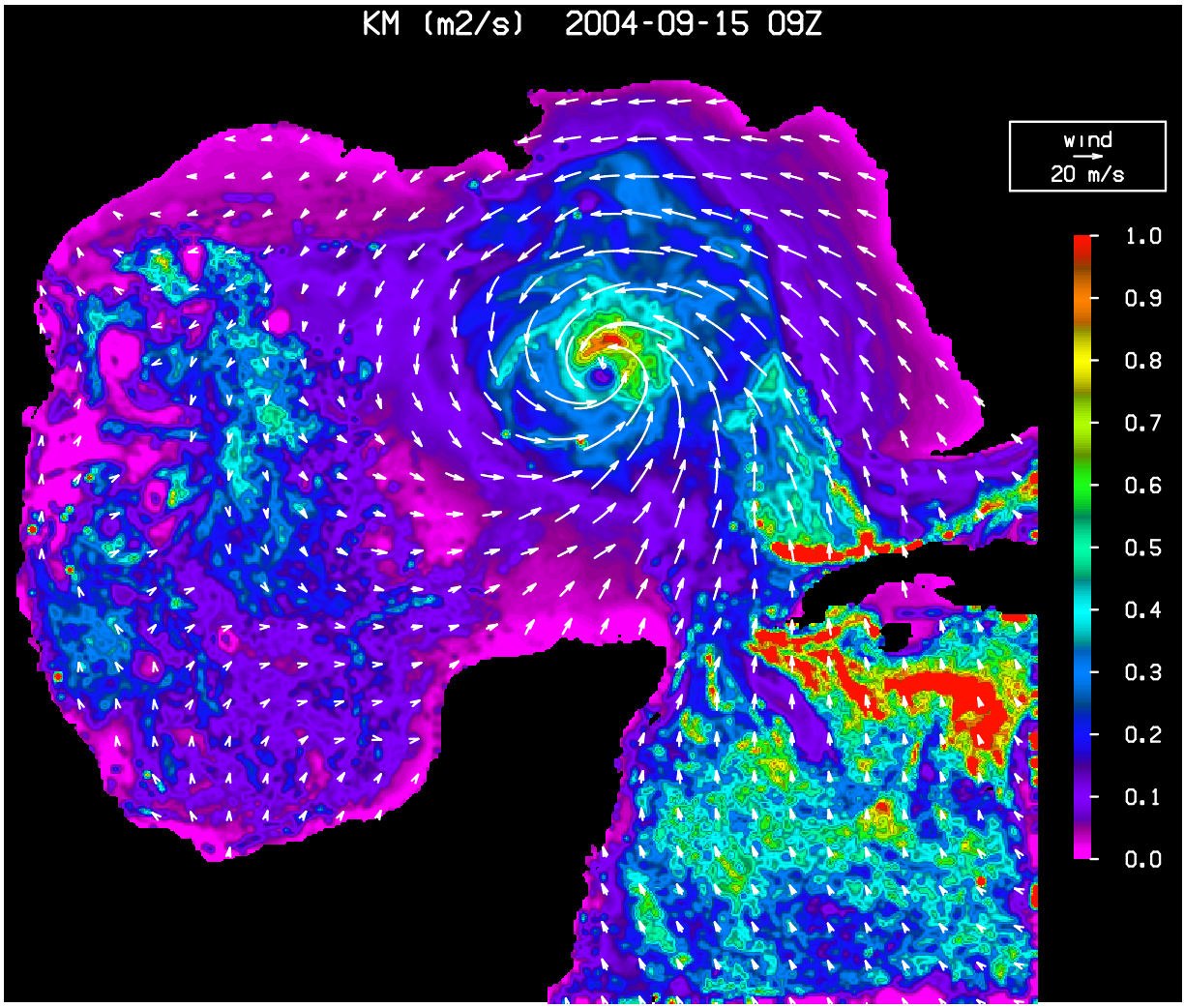

Fig. 19 — Maximum value of K_M in SML for Hurricane Ivan simulations with KC04 LCMP at 09Z 15 September 2004. The white vectors show the surface winds.

night-time convective mixing occurring in some areas, e.g., in the western GoM and the northwest Caribbean. On the afternoon of September 15 (local time), most of this mixing is significantly reduced due to day-time solar heating (not shown). However, the mixing near the hurricane is primarily wind-driven and remains strong through the day and night. Also, the stronger mixing south of and just north of Cuba is partly due to this area being on the warm side of the Loop Current where the SML is generally deeper than on the cold side.

Figure 20 shows the ratio of the spatially-filtered values of the maximum value of K_M in the SML for the simulations with the H15 LCMP and without a LCMP at 09Z 15 September 2004. Near the hurricane, the ratios range from about 1 to 10. This indicates that the H15 LCMP is significantly increasing the mixing rates in the areas of strong hurricane winds. The areas where the ratio is below one are generally occurring in areas of night-time convection.

Figure 21 shows the ratio of the spatially-filtered values of the maximum value of K_M in the SML for the simulations with the KC04 LCMP and without a LCMP at 09Z 15 September 2004. Near the hurricane, the ratios range from 1 to 4 and are frequently in the range of 2 to 3. This indicates that the KC04 scheme is significantly increasing the mixing rates in the areas of strong hurricane winds, though not nearly as much as the H15 LCMP. The areas where the ratio is below one are generally occurring in areas of night-time convection.

6. SUMMARY

Mellor-Yamada-type turbulence models have long been criticised for not mixing the ocean's surface layer strongly or deeply enough in the open ocean. Recent LES simulations of Langmuir circulation in the upper ocean, e.g., MW97, found that the occurrence of LCs significantly increases the net rate of mixing within the SML and slightly increases the MLD. The original Mellor-Yamada-type turbulence models did not account for these effects.

Based on the LES results of MW97, KC04 parameterized and tested the effects of enhanced mixing by LC in the MYL2.5 turbulence model. KC04 parameterized the effect of LC mixing in the MYL2.5 turbulence model by adding additional shear-production terms to the TKE and TLS equations of the turbulence model. These additional terms consist of the product of the vertical turbulent momentum flux and the vertical shear of the SDC from the surface wave field.

H15 noted that KC04 were not fully consistent in their application of the CL vortex force to the ARSM used derive the MYL2.5 turbulence model, and derived alternative modifications to the turbulence model to account for the enhancment of vertical mixing by LC. This included modifications to the representation of the vertical turbulent momentum fluxes, which are used in the mean horizontal momentum equations as well as in the turbulence model's TKE and TLS equations, and to the stability functions of the turbulence model.

Both the KCO4 and H15 LCMPs were implemented in the MYL2.5 turbulence model used in NCOM and tested by conducting simulations of the simple, light-wind, mixing case used by MW97 (and also by KC04 for their own testing), the upper-ocean thermal structure at OWS Papa during 1961, and Hurricane Ivan in the Gulf of Mexico in 2004.

The simple test case used by MW97 and KC04 consisted of forcing by a constant surface wind stress of 0.037 Pa (which corresponds to a wind speed of about 5 m/s), a small, cooling surface heat

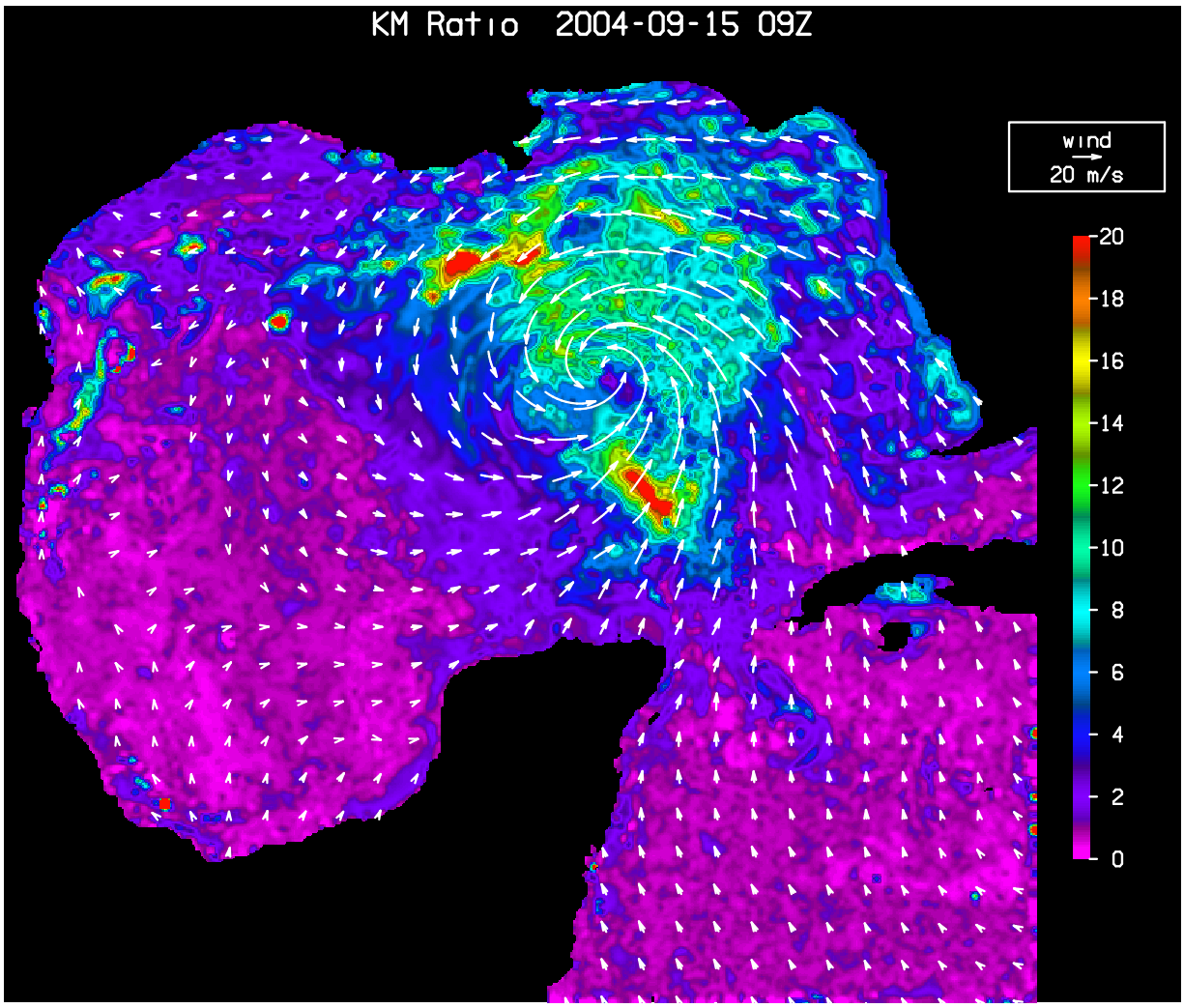

Fig. 20 — Ratio of maximum values of K_M in SML for Hurricane Ivan simulations with the H15 LCMP and without a LCMP at 09Z 15 September 2004. The white vectors show the surface winds.

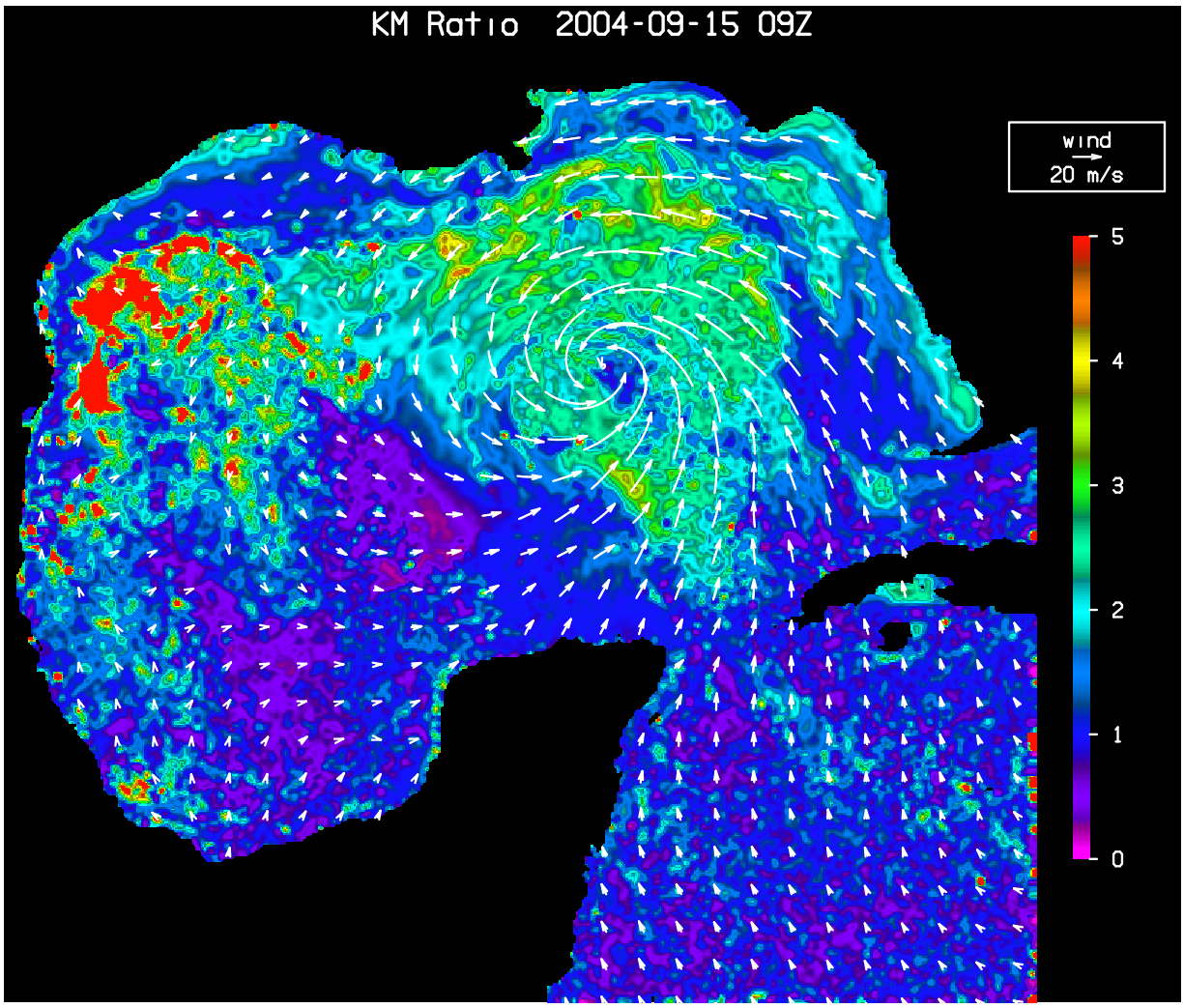

Fig. 21 — Ratio of maximum values of K_M in SML for Hurricane Ivan simulations with the KC04 LCMP and without a LCMP at 09Z 15 September 2004. The white vectors show the surface winds.

flux of 5 W/m^2, and an initial MLD of 33 m. The use of the KC04 LCMP increased the maximum rate of mixing in the SML by about a factor of two from about 200 to 400 m^2/s, and increased the MLD by about 3 m. The increase in the maximum rate of mixing from LC was roughly consistent with the results in MW97 and KC04. The use of the H15 LCMP resulted in a similar increase in the MLD of about 3 m, but increased the maximum rate of mixing in the SML to a value of about 1500 m^2/s.

For the Papa simulations for 1961, no direct wave observations were available. Hence, the wave field was estimated from the Papa winds by establishing a relation between the local wind speed and the wave spectrum based on 9 years of wind and wave observations from NOAA Buoy 46005, located in the northeast Pacific about 1100 km SE of OWS Papa.

The use of the KC04 LCMP at Papa increased the rate of mixing within the SML in the spring and summer by about a factor of 2 over the original MYL2.5 MLM without a LCMP. The predicted MLD at Papa was slightly increased, but not enough to provide good agreement with the observed MLD in the summer and fall of 1961. However, addition of the L94 parameterization of unresolved mixing processes (Large et al. 1994) deepened the ML enough to provide good agreement with the observed MLD at Papa. This was consistent with KC94, who reported that their implementation of L94 in the MYL2.5 turbulence model significantly improved the predicted MLD at Papa.

The simulation at Papa with the H15 LCMP resulted in a fairly good prediction of the observed SST, MLD, and ISODs without the need to incorporate additional mixing mechanisms, e.g., such as the L94 parameterization. The H15 LCMP increased the rate of mixing within the SML in the spring and summer at Papa by about a factor of 2–5 over the rates of mixing predicted by the KC04 LCMP; hence, about a factor of 4–10 over the original MYL2.5 MLM.

For the simulations of Hurricane Ivan in the Gulf of Mexico, the use of the KC04 and H15 LCMPs generally resulted in significantly increased mixing rates in the SML near the hurricane, i.e., the mixing rates are increased by a factor of 2 to 3 for KC04 and by a factor of 5 to 10 for H15. The increased mixing rates result in a significant reduction in the vertical shear of the wind-driven currents in the SML, which results in a reduction of the surface value of the wind-driven current near the hurricane of 20 cm/s or more. The depth of mixing is also generally increased, which results in increased cooling of the SST. For the KC04 LCMP the additional SST cooling is small, i.e., generally less than 0.2°C; but for H15 the increased cooling is greater, i.e., 0.2–0.4°C.

7. ACKNOWLEDGMENTS

Thanks to Lakshmi Kantha and to Ramsey Harcourt for very helpful discussions regarding the implementation of their parameterizations of Langmuir circulation mixing in the Mellor-Yamada Level 2.5 turbulence model. Thanks to Jim Dykes of NRL for providing the COAMPS atmospheric forcing fields for Hurricane Ivan, and to Erick Rogers of NRL for providing the SWAN wave forcing fields for Hurricane Ivan. This work was funded through the 6.2 NRL Core Project "Coupled Ocean-Wave Prediction System,", through the 6.2 NRL Core Project "Full Column Mixing for Numerical Ocean Models", and through the 6.1 NRL project "Remote sensing of the upper ocean mixing induced by Langmuir turbulence".

8. REFERENCES

Barron, C.N., A.B. Kara, H.E. Hurlburt, C. Rowley, and L.F. Smedstad (2004). "Sea Surface Height Predictions from the Global Navy Coastal Ocean Model (NCOM) During 1998–2001," *J. Atmos. Oceanic Technol.* **21**(12), 1876–1894.

Booij, N., R.C. Ris, and L.H. Holthuijsen (1999). "A Third-Generation Wave Model for Coastal Regions: 1. Model Description and Validation," *J. Geophys. Res.* **104**(C4), 7649–7666.

Carniel, S., M. Sclavo, L.H. Kantha, and C.A. Clayson, 2005: Langmuir cells and mixing in the upper ocean. *Il Nuovo Cimento*, **28**, 33–54.

Charnock, H. (1955). "Wind Stress on a Water Surface," *Quart. J. Roy. Meteor. Soc.* **81**, 639–640.

Chen S., T.J. Campbell, S. Gabersek, R.M. Hodur, and P.J. Martin (2010). "Effect of two-way air-sea coupling in high and low wind speed regimes," *Mon. Wea. Rev.* **138** No. 9, 3579–3602.

Craig, P.D. and M.L. Banner (1994). "Modeling Wave-enhanced Turbulence in the Ocean Surface Layer," *J. Phys. Oceanogr.* **24**, 2546–2559.

Denman, K.L. and M. Miyake (1973). "Upper Layer Modification at Ocean Station Papa: Observations and Simulation," *J. Phys. Oceanogr.* **3**, 185–196.

Gaspar, P. (1988). "Modeling the Seasonal Cycle of the Upper Ocean," *J. Phys. Oceanogr.* **18**, 161–180.

Grant, W.D. and O.S. Madsen (1979). "Combined Wave and Current Interaction with a Rough Bottom," *J. Geophys. Res.* **84**, 1979–1808.

Harcourt, R. (2013). "A second moment closure model of Langmuir turbulence," *J. Phys. Oceanogr.* **43**(4), 673–697. doi: 10.1175/JPO-D-12-0105.1

Harcourt, R.R. (2015). "An Improved Second-Moment Closure Model of Langmuir Turbulence," *J. Phys. Oceanogr.* **45**, 84–103.

Hodur, R.M. (1997). "The Naval Research Laboratory's Coupled Ocean/Atmosphere Mesoscale Prediction System (COAMPS)," *Mon. Wea. Rev.* **125**, 1414–1430.

Jerlov, N. G. (1968). *Optical Oceanography* (Elsevier Publ. Co., Inc., New York), 194 pp.

Kantha L.H. and C.A. Clayson (1994). "An Improved Mixed Layer Model for Geophysical Applications," *J. Geophys. Res.* **99**, 25235–25266.

Kantha L.H. and C.A. Clayson (2004). "On the Effect of Surface Gravity Waves on Mixing in the Oceanic Mixed Layer," *Ocean Modelling* **6**, 101–124.

Large, W.G. (1996). "An Observational and Numerical Investigation of the Climatological Heat and Salt Balances at OWS Papa," *J. Climate* **9**, 1856–1876.

Large, W.G., J.C. McWilliams, and S. Doney (1994). "Oceanic Vertical Mixing: a Review and a Model with a Nonlocal Boundary Layer Parameterization," *Rev. Geophys.* **32**, 363–403.

Levitus, S. (1982). "Climatological Atlas of the World Ocean," NOAA Prof. Paper 13, U.S. Govt. Print Office, Washington, D.C., 173 pp.

Li, M., C. Garrett, and E. Skyllingstad (2005). "A Regime Diagram for Classifying Turbulent Large Eddies in the Upper Ocean," *Deep-Sea Res.* **52**, 259–278.

Martin, P. J. (1982). "Mixed-Layer Simulation of Buoy Observations Taken During Hurricane Eloise." *J. Geophys. Res.* **87**, 409–427.

Martin, P. J. (1985). "Simulation of the Mixed Layer at OWS N and P with Several Models," *J. Geophys. Res.* **90**, 903–916.

Martin, P. J. (1986). "Testing and Comparison of Several Mixed-Layer Models," NORDA Report 143. Naval Research Laboratory, Stennis Space Center, MS 39529, 30 pp.

Martin, P.J., and R.A. Allard (1993), "The calculation of solar extinction from satellite color for ocean modelling." NRL Memorandum Report NRL/MR/7322–93-7021, Naval Research Laboratory, SSC, MS 39529, 64 pp.

Martin, P.J. (2000). "A Description of the Navy Coastal Ocean Model Version 1.0," NRL Report NRL/FR/7322–00-9962, Naval Research Laboratory, SSC, MS 39529, 42 pp.

Martin, P.J., E. Rogers, R.A. Allard, P.J. Hogan, and J.G. Richman (2012). "Results from Tests of Direct Wave Mixing in the Ocean's Surface Mixed Layer." NRL Report NRL/FR/7322–12-10216, Naval Research Laboratory, SSC, MS 39529, 35 pp.

Martin, P.J., E. Rogers, R.A. Allard, J.D. Dykes, and P.J. Hogan (2013). "Tests of Parameterized Langmuir-Circulation Mixing in the Ocean's Surface Mixed Layer," NRL Memorandum Report NRL/MR/7320–13-9444, Naval Research Laboratory, SSC, MS 39529, 47 pp.

Martin, P.J., and P.J. Hogan (2013). "Tests of vertical mixing in NCOM," Unpublished Report, Naval Research Laboratory, SSC, MS 39529, 15 pp.

McWilliams, J.C., P.P. Sullivan, and C.-H. Moeng (1997). "Langmuir Turbulence in the Ocean." *J. Fluid Mech.* **334**, 1–30.

Mellor, G.L. and A. Blumberg (2004). "Wave Breaking and Ocean Surface Layer Thermal Response." *J. Phys. Oceanogr.* **34**, 693–698.

Mellor, G.L. and P.A. Durbin (1975). "The Structure and Dynamics of the Ocean Surface Mixed Layer," *J. Phys. Oceanogr.* **5**, 718–728.

Mellor, G.L. and T. Yamada (1974). "A Hierarchy of Turbulence Closure Models for Planetary Boundary Layers," *J. Atmos. Sci.* **31**, 1791–1806.

Mellor, G.L. and T. Yamada (1982). "Development of a Turbulence Closure Model for Geophysical Fluid Problems," *Geophys. and Space Phys.* **20**, 851–875.

Morey, S.L., P.J. Martin, J.J. O'Brien, A.A. Wallcraft, and J. Zavala-Hidalgo (2003). "Export Pathways for River Discharged Fresh Water in the Northern Gulf of Mexico," *J. Geophys. Res.*, **108**, 1–15.

Price, J.F. (1981). "On the Upper-Ocean Response to a Moving Hurricane," *J. Phys. Oceanogr.* **11**, 153–175.

Rosmond, T.E., J. Teixeira, M. Peng, T.F. Hogan, and R. Pauley (2002), "Navy Operational Global Atmospheric Prediction System (NOGAPS): Forcing for Ocean Models," *Oceanography* **15**, 99–108.

Skyllingstad, E.D., and D.W. Denbo (1995). "An Ocean Large-Eddy Simulation of Langmuir Circulations and Convection in the Surface Mixed Layer," *J. Geophys. Res.* **100**, 8501–8522.

Soulsby, R.L. (1995). "Bed Shear-Stresses Due to Combined Waves and Currents," in *Advances in Coastal Morphodynamics*, edited by M. Stive, J. Fredsoe, L. Hamm, R. Soulsby, C. Teisson, and J. Winterwerp, Delft Hydraulics, Delft, The Netherlands, 420–423.

Troen, I.B., and L. Mahrt (1986), "A simple model of the atmospheric boundary layer; sensitivity to surface evaporation," *Boundary Layer Meteorol.* **37**, 129–148.

Appendix A

CALCULATION OF SDC FOR A MONOCROMATIC WAVE

The Stokes drift current (SDC) V_s can be computed for a monocromatic (i.e., single frequency) wave using

$$V_s(z) = (ak)^2 c_p \frac{\cosh(2k(H+z))}{2\sinh^2(kH)}, \tag{A1}$$

where a is the wave amplitude, $k = 2\pi/L$ is the wavenumber, L is the wavelength, $c_p = (\tanh(kH)g/k)^{\frac{1}{2}}$ is the phase speed, g is the acceleration of gravity, H is the total water depth, and z is the distance to the surface.

In deep water, this simplifies to

$$V_s(z) = (ak)^2 c_p \exp(2kz), \tag{A2}$$

where the phase speed is $c_p = (g/k)^{\frac{1}{2}}$.

For a wave field consisting of waves of different amplitudes, frequencies, and directions, the contributions to the SDC from the different waves can be summed (in a vector sense).

The wave amplitude a is related to the wave energy E as

$$E = \frac{1}{2}a^2. \tag{A3}$$

Note that the wave energy given by Eq. (A3) has units of length squared, which is a common practice when discussing surface waves. Multiplication by the water density and the acceleration of gravity gives the proper units of energy per m^2 of surface area.

Appendix B

CALCULATION OF SDC USING WAVE SPECTRA FROM NOAA BUOY

Some of the NOAA buoys provide observations of both the surface wind velocity and the wave energy spectra. These data allow the calculation of the average wave spectra at different wind speeds. The average wave spectra at the different wind speeds can then be used to estimate the SDC for a given wind speed.

The spectral wind and wave data that were used here were from NOAA Buoy 46005, which is located in the northeast Pacific at 131.001°W, 46.100°N, which is about 1100 km east-southeast of the location of OWS Papa. Since the location of the buoy is somewhat similar to that of OWS Papa, the wind and wave conditions should be roughly similar.

Data from Buoy 46005 for the years 1996 through 2004 were used. For these years, the spectral wave data from the buoy consist of 38 values of the wave energy at frequencies from 0.03 to 0.4 Hz at 0.01 Hz intervals. Note that no directional information is provided for the wave data from Buoy 46005. Averages of the spectral data were computed within 1-m/s-wide wind-speed bins from 1 to 20 m/s. No winds above 20 m/s were recorded at Buoy 46005 during the 9-year period. The wind speed used to characterize the wave spectrum in this calculation is the wind speed at the time of the wave observation. An alternative would be to use some time-weighted wind speed over the previous few hours, but this was not done.

Figure B1 shows the averaged wave spectra from NOAA Buoy 46005 for wind speeds of 1, 5, 10, 15, and 20 m/s. The wave energy increases with increasing wind speed. There are, however, a couple of notable aspects to the wave spectra in Fig. B1: (1) the location of the peak of the wave energy spectra shows little change with wind speed, and (2) there is a notable amount of wave energy present at low wind speeds of 1 to 5 m/s.

There are several limitations to estimating the SDC from a wave spectra based on the current local wind velocity. The wind duration and fetch and the propagation of waves from other areas cannot be accounted for. Additionally, variation in the direction of the waves making up the energy spectrum cannot be accounted for; hence, the direction of the waves and the SDC is assumed to be downwind.

The SDC profiles estimated from the wave spectra at Buoy 46005 for different wind speeds were compared with the SDC profiles computed from the observed wave spectra using data for the year 2000, and the mean and rms differences versus depth are shown in Fig. B2. The SDC estimated by this method will be referred to in this report as the Buoy Wave Spectra (BWS) SDC. Plots for the same errors computed using data from buoy 46005 for other years between 1996 and 2004 (not shown) look similar to Fig.B2.

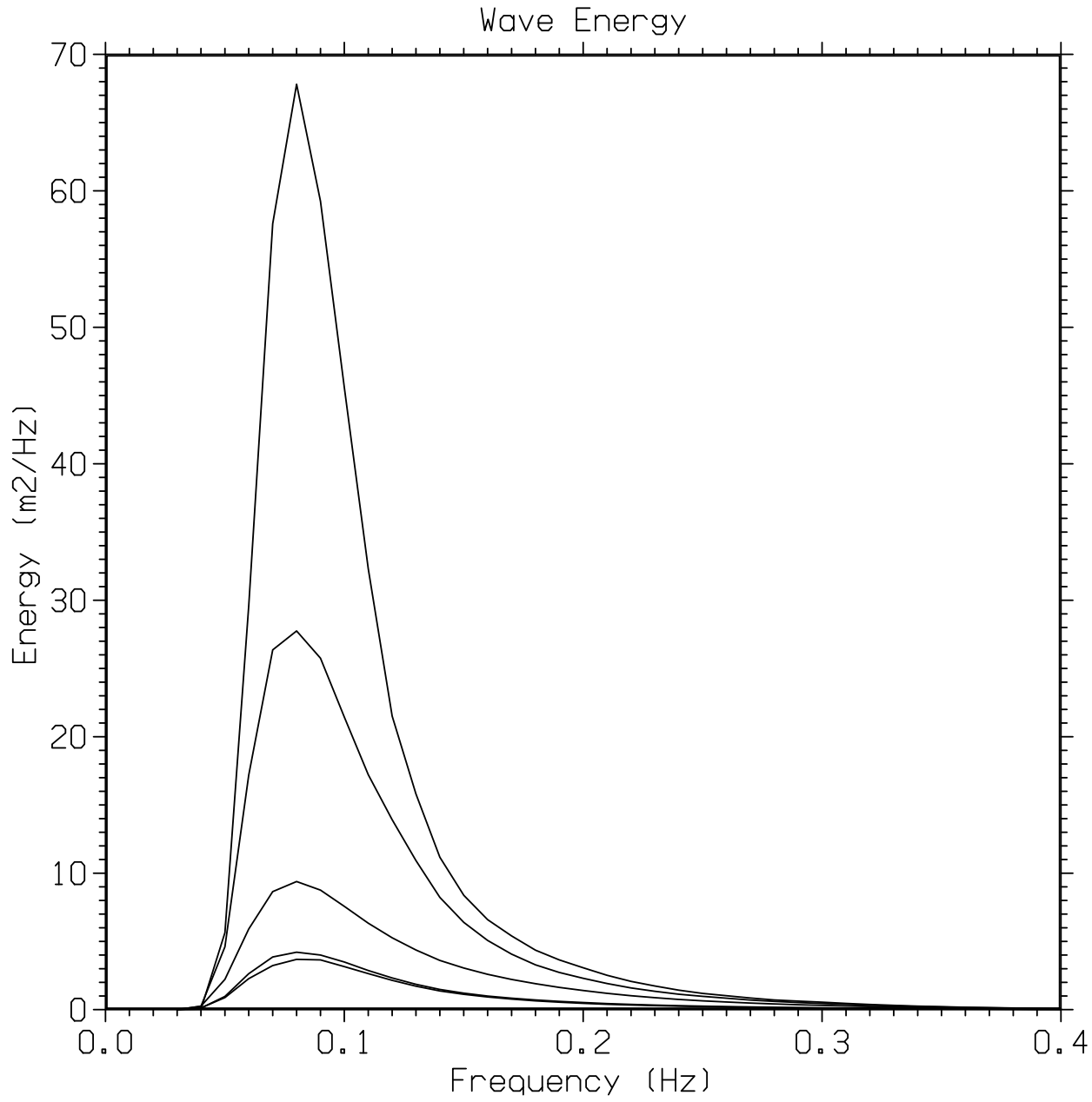

Fig. B1 — Averaged wave spectra from NOAA Buoy 46005 for wind speeds of 1, 5, 10, 15, and 20 m/s. The wave energy increases with wind speed.

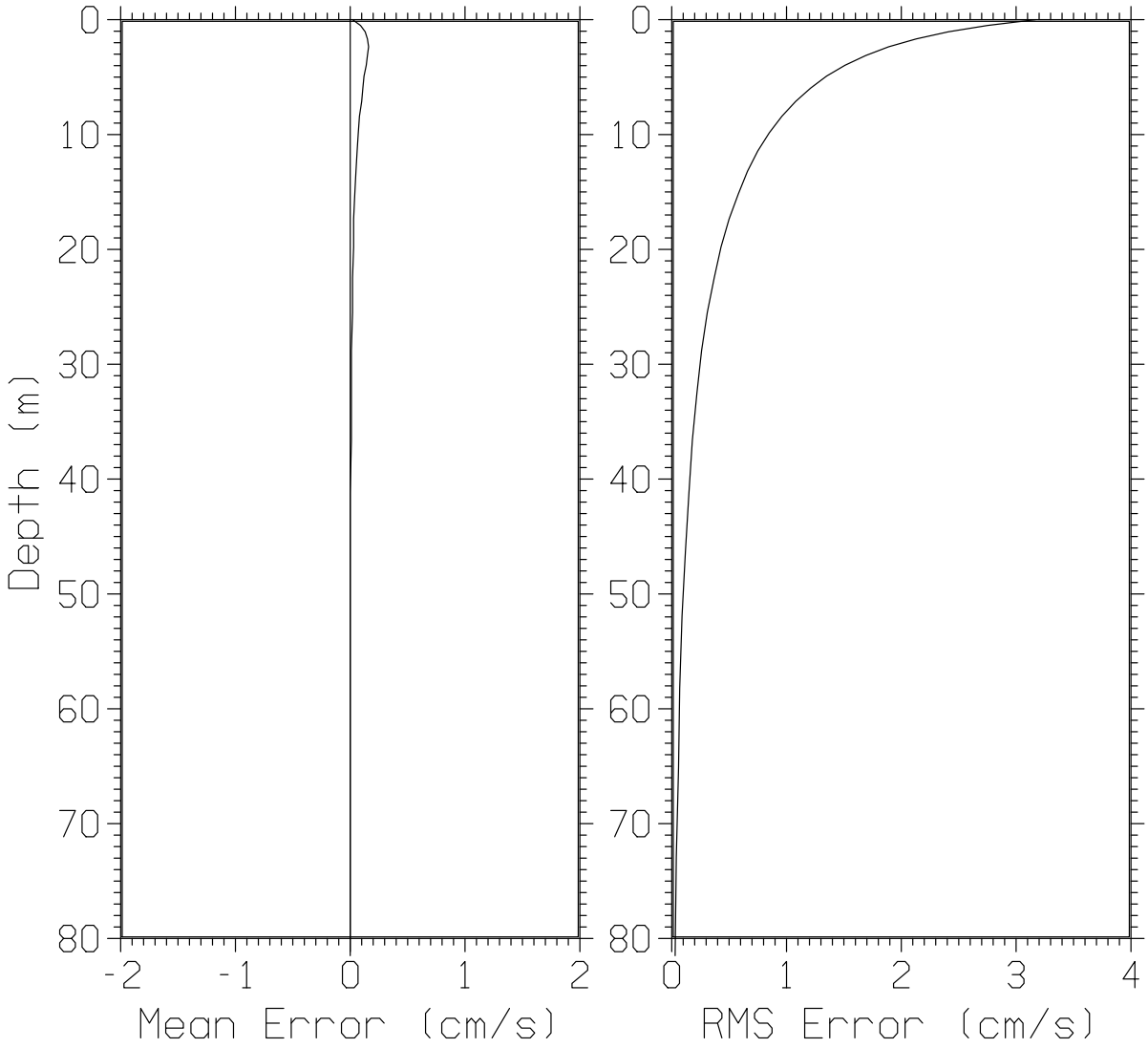

Fig. B2 — Mean and RMS errors for the BWS-computed SDC at buoy 46005 for the year 2000. Errors are with respect to the SDC computed from the observed wave spectra at buoy 46005 for the year 2000.

Appendix C

PARAMETERIZATION OF UNRESOLVED MIXING PROCESSES BY LARGE ET AL. (1994)

As noted in the introduction to this report, tests of upper-ocean mixing in the open ocean with turbulence models such as the MYL2.5 MLM have frequently found that the models do not predict as much mixing as is observed. It has been hypothesized that is due, not so much to the fact that the mixing mechanisms in the models are incorrect, but that some mixing processes are either unrepresented or under-represented, including sources of background shear (e.g., internal waves and inertial gravity wave pumping), surface waves, and Langmuir circulation.

To account for shear instability mixing below the SML, Large et al. (1994, referred to in this report as L94) proposed extending such mixing to Richardson numbers R_i above the normal critical value of 0.2 to 0.3, where shear instability is suppressed by the strength of the density stratification. The L94 mixing enhancement extends the mixing to $R_i = 0.7$ and is described by

$$K_{L94} = \begin{array}{lll} K_o & & R_i < 0 \\ K_o(1-(R_i/0.7)^2)^3 & 0 < R_i & < 0.7 \\ 0 & & R_i > 0.7, \end{array}$$

where $K_o = 50$ cm^2/s. In NCOM, K_{L94} is computed from R_i and is applied to the vertical mixing of the momentum and scalar fields (e.g., temperature and salinity) by using the maximum of the usual vertical mixing coeffient (K_M or K_H for momentum or scalar fields, respectively) and K_{L94} to compute the vertical mixing.

This scheme was utilized by L94 in conjunction with an adaptation of the atmospheric boundary layer model of Troen and Mahrt (1986) to the ocean (known as the KPP MLM), and by Kantha and Clayson (1994, referred to in this report as KC94) in conjunction with the MYL2.5 turbulence closure model. Both L94 and KC94 found that the addition of this mixing improved the agreement of predictions of the ocean surface mixed layer with observations from several open-ocean data sets, including data from OWS Papa. However, a question is whether such a mixing enhancement is needed in shallow, coastal water, where overmixing is sometimes more of a problem than undermixing.